OXFORD

Human Molecular Genetics, 2015, Vol. 24, No. 21 6213–6228

doi: 10.1093/hmg/ddv339
Advance Access Publication Date: 24 August 2015
Original Article

ORIGINAL ARTICLE

Distinct expression and function of whirlin isoforms in the inner ear and retina: an insight into pathogenesis of USH2D and *DFNB31*

Pranav Dinesh Mathur[1,2], Junhuang Zou[1], Tihua Zheng[1], Ali Almishaal[3], Yong Wang[4], Qian Chen[1], Le Wang[1,5], Deepti Vashist[1], Steve Brown[6], Albert Park[4] and Jun Yang[1,2,4,*]

[1]Department of Ophthalmology and Visual Sciences, Moran Eye Center, University of Utah, 65 Mario Capecchi Drive, Salt Lake City, UT 84132, USA, [2]Department of Neurobiology and Anatomy, University of Utah, 20 North 1900 East, Salt Lake City, UT 84132, USA, [3]Department of Communication Sciences and Disorders, University of Utah, 390 South 1530 East, Salt Lake City, UT 84112, USA, [4]Division of Otolaryngology, Department of Surgery, University of Utah, 50 North Medical Drive, Salt Lake City, UT 84132, USA, [5]The First Affiliated Hospital, Jilin University, Changchun, Jilin 130061, China and [6]Mammalian Genetics Unit, Medical Research Council, Harwell, Oxfordshire OX11 ORD, UK

*To whom correspondence should be addressed at: John A Moran Eye Center, University of Utah, 65 Mario Capecchi Drive, Bldg 523, Salt Lake City, UT 84132, USA. Tel: +1 8012132591; Email: jun.yang@hsc.utah.edu

Abstract

Usher syndrome (USH) is the most common inherited deaf-blindness with the majority of USH causative genes also involved in nonsyndromic recessive deafness (DFNB). The mechanism underlying this disease variation of USH genes is unclear. Here, we addressed this issue by investigating the *DFNB31* gene, whose mutations cause USH2D or *DFNB31* depending on their position. We found that the mouse *DFNB31* ortholog (*Dfnb31*) expressed different mRNA variants and whirlin protein isoforms in the cochlea and retina, where these isoforms played different roles spatially and temporally. Full-length (FL-) whirlin in photoreceptors and hair cell stereociliary bases is important for the USH type 2 protein complex, while FL- and C-terminal (C-) whirlins in hair cell stereociliary tips participate in stereociliary elongation. Mutations in the whirlin N-terminal region disrupted FL-whirlin isoform in the inner ear and retina but not C-whirlin in the inner ear, and led to retinal degeneration as well as moderate to severe hearing loss. By contrast, a mutation in the whirlin C-terminal region eliminated all normal whirlin isoforms but generated a truncated N-terminal whirlin protein fragment, which was partially functional in the retina and thus prevented retinal degeneration. Mice with this mutation had profound hearing loss. In summary, disruption of distinct whirlin isoforms by *Dfnb31* mutations leads to a variety of phenotype configurations and may explain the mechanism underlying the different disease manifestations of human *DFNB31* mutations. Our findings have a potential to improve diagnosis and treatment of USH disease and quality of life in USH patients.

Introduction

Usher syndrome (USH) is an incurable autosomal recessive genetic disease. It is manifested as combined congenital or progressive hearing loss and progressive retinal degeneration. Some patients also have balance dysfunction. This disease accounts for the majority of deaf-blindness cases, with a prevalence of 1 in 6000 people in the world (1). Currently, approximately 10 USH causative and modifier genes have been identified (2). Among these genes,

Received: June 22, 2015. **Revised and Accepted:** August 17, 2015

nine are also associated with other diseases with the most common one being nonsyndromic recessive deafness (DFNB) (2). The involvement of USH genes in multiple diseases yields uncertainty for early accurate diagnosis, which is crucial for timely treatment and education of patients in preparation for the onset of symptoms at a later age, such as retinal degeneration. However, the molecular mechanisms underlying these distinct disease manifestations caused by mutant USH genes are poorly understood. Genotype–phenotype correlations are proposed, although non-genetic factors and/or unknown modifier genes may also be involved. For example, nonsense, frameshift, and some splice site mutations of harmonin, cadherin 23, and protocadherin 15 genes have been found to cause USH. Conversely, missense and some other splice site mutations of these genes are associated with DFNB, probably due to their residual functions (3–5). Additionally, most USH genes express multiple alternatively spliced protein isoforms, which may have different functions in the inner ear and retina (6–13). Disruption of the different isoforms of the same genes may also contribute to the genotype–phenotype correlations found in USH patients (14,15).

DFNB31 is the causative gene of USH2D (OMIM: 611383) (14,16,17) and *DFNB31* subtypes (OMIM: 607084) (18,19) (Fig. 1A). There appears to be a correlation between the mutation position and disease manifestation. Mutations leading to premature translation termination at whirlin protein N- and C-terminal regions tend to cause USH2D and *DFNB31*, respectively. This genotype–phenotype correlation was also observed in mice (Fig. 1A). Two *Dfnb31* (also known as *Whrn* in mice) mutant mouse lines have been phenotypically characterized in detail (18,20,21). $Dfnb31^{neo/neo}$ mice, generated by replacing 3′ part of *Dfnb31* first exon with a Neo^r cassette, exhibit hearing loss and late-onset retinal degeneration. On the other hand, $Dfnb31^{wi/wi}$ mice with a spontaneous deletion between *Dfnb31* exons 6–9 are deaf but do not develop retinal degeneration. Up to now, the exact underlying molecular mechanism is unclear. *Dfnb31* encodes multiple whirlin isoforms derived from alternative splicing and usage of promoters in the inner ear and retina (11,22). It has been postulated that disruption of distinct isoforms by *DFNB31* mutations is the cause of USH2D and *DFNB31* manifestations (14,20). However, direct experimental evidence supporting this mechanism is still missing.

In inner ear hair cells, whirlin isoforms are localized to the stereociliary tips of mechanosensitive hair bundles and are required for normal stereociliary elongation (11). Whirlin isoforms are also present at the base of stereocilia as a component of the ankle link complex (23). In retinal photoreceptors, whirlin isoforms participate in organizing the periciliary membrane complex at the inner segment apex just beneath the outer segment, the organelle for phototransduction (20,24). However, it is unclear which exact whirlin protein isoforms are expressed in these tissues and what the specific subcellular localizations and functions of these isoforms are. The lack of this important information hinders development of therapies for USH2D and *DFNB31*, especially the viral-mediated gene replacement therapy. Additionally, understanding the functions of individual whirlin isoforms will provide novel insights into the molecular mechanisms underlying stereociliary bundle development, which is essential for stem cell-based regeneration of hair cells with functional stereociliary bundles.

In this study, we utilized the two well-characterized ($Dfnb31^{neo/neo}$ and $Dfnb31^{wi/wi}$ mice) and two additional ($Dfnb31^{tm1a/tm1a}$ and $Dfnb31^{wi/wi}$-BAC mice) *Dfnb31* mouse models. We show for the first time that the expression and localization of whirlin isoforms are different in the cochlea and the retina. These different whirlin isoforms have distinct functions in the respective tissues. We further present evidence that whirlin mutations at different gene positions disrupt the expression of whirlin isoforms differentially and thus lead to different combinations of inner ear and retinal phenotypes.

Results

Expression of *Dfnb31* mRNA variants in the inner ear and retina of wild-type, $Dfnb31^{neo/neo}$ and $Dfnb31^{wi/wi}$ mice

We studied the eleven *Dfnb31* mRNA variants that have so far been identified from the mouse inner ear and retina (Fig. 1B) (11,22). These *Dfnb31* mRNA variants are categorized into four groups with minor amino acid differences among variants within each group. Group 1 including variants 1–4 is translated into full-length whirlin isoforms (FL-whirlin) carrying three PDZ domains and one proline-rich region. Variants 5–7 in Group 2 share the same promoter region with Group 1, but are alternatively spliced to skip 3′ part of exon 1 and either exons 2–5 or exons 2–6. This group of variants is predicted to be translated into proteins with only the proline-rich region and third PDZ domain (C-whirlin). Variants 8–9 in Group 3 utilize alternative promoters in intron 5 and can be translated into proteins similar to Group 2 proteins (C-whirlin). Groups 1–3 of *Dfnb31* mRNA variants were identified from the mouse vestibular system (11). The fourth group of *Dfnb31* mRNA variants (10–11) was found in mouse retinas (22). Alternative splicing after exon 4 or 7 in this group leads to short *Dfnb31* transcripts, which are thought to be translated into protein isoforms with only N-terminal one or two PDZ domains (N-whirlin).

We designed primers specific to each group of *Dfnb31* mRNA variants (Fig. 1B and Supplementary Material, Table S1) and characterized the expression of these variants by RT–PCR using total RNA isolated from the adult mouse retina and P4 mouse cochlea. In the wild-type retina, groups 1, 3 and 4 of *Dfnb31* mRNA variants were detected but not group 2 (Fig. 1C). Groups 1 and 3 of *Dfnb31* variants were truncated between exons 6-9 in $Dfnb31^{wi/wi}$ retinas, while all other *Dfnb31* variants were absent in $Dfnb31^{neo/neo}$ and $Dfnb31^{wi/wi}$ retinas (Fig. 1C). The truncated group 1 *Dfnb31* variants in $Dfnb31^{wi/wi}$ mice can be translated into N-whirlin fragments (hereafter referred to as truncated N-whirlin) with amino acid sequences similar but not identical to those of the normal N-whirlin isoforms translated from group 4 variants (Fig. 1D), while the truncated group 3 variant is probably unable to be translated into a functional protein (Fig. 1D). The reason underlying the difference between the RT–PCR results using primer pairs a/d and c/d for group 1 whirlin variants in $Dfnb31^{wi/wi}$ mice is unclear (Fig. 1C). Probably, an alternative 5′ sequence exists in the group 1 *Dfnb31* variants of $Dfnb31^{wi/wi}$ mice. In the wild-type cochlea, variants in group 1 as well as variant 8 were expressed (Fig. 1C). In the $Dfnb31^{neo/neo}$ cochlea, variant 8 was intact, while others were undetectable (Fig. 1C and D). In the case that an aberrant *Dfnb31* transcript lacking only exon 1 was expressed in $Dfnb31^{neo/neo}$ inner ears, we analyzed the nucleotide sequence of this potential aberrant transcript and could not find an inframe translation start codon except the one used in variant 8. Therefore, if this aberrant transcript existed in $Dfnb31^{neo/neo}$ inner ears, it could only be translated into a protein identical to C-whirlin. The $Dfnb31^{wi/wi}$ mutation truncated variants 1–4 and 8 in the cochlea (Fig. 1C and D), which is the same as in the retina.

Localization of whirlin protein isoforms in the cochlear hair cells of wild-type, $Dfnb31^{neo/neo}$ and $Dfnb31^{wi/wi}$ mice

Based on the RT–PCR results, we predicted that FL- and C-whirlin proteins could exist in the wild-type cochlea, C-whirlin protein in

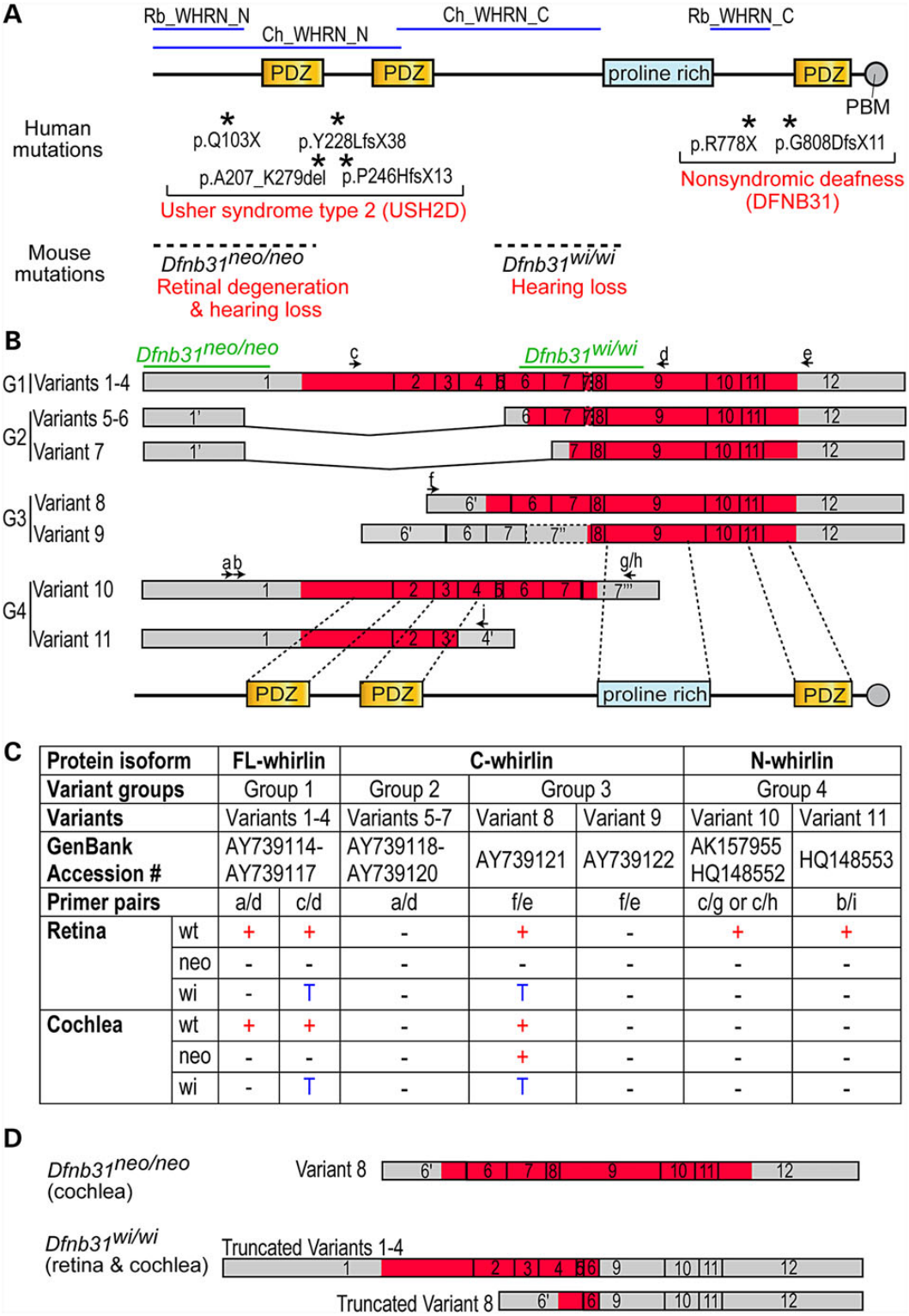

Protein isoform		FL-whirlin		C-whirlin			N-whirlin	
Variant groups		Group 1		Group 2	Group 3		Group 4	
Variants		Variants 1-4		Variants 5-7	Variant 8	Variant 9	Variant 10	Variant 11
GenBank Accession #		AY739114-AY739117		AY739118-AY739120	AY739121	AY739122	AK157955 HQ148552	HQ148553
Primer pairs		a/d	c/d	a/d	f/e	f/e	c/g or c/h	b/i
Retina	wt	+	+	-	+	-	+	+
	neo	-	-	-	-	-	-	-
	wi	-	T	-	T	-	-	-
Cochlea	wt	+	+	-	+	-	-	-
	neo	-	-	-	+	-	-	-
	wi	-	T	-	T	-	-	-

Figure 1. *DFNB31/Dfnb31* genotype–phenotype correlation and disruption of *Dfnb31* mRNA variants in *Dfnb31* mutant mice. (**A**) Mutations in the N- and C-terminal whirlin regions cause different diseases in humans (asterisks and upper red text) and phenotypes in mice (dashed lines and lower red text). Blue lines on the top mark the antigen regions of various whirlin antibodies used in this study. (**B**) Schematic diagram of various *Dfnb31* mRNA variants reported in the mouse inner ear and retina (11,22). Arabic numerals are exon numbers. Gray and red colors indicate untranslated and protein coding regions, respectively. Arrows and lower case letters show the position, direction, and name of primers used for RT–PCR experiments. The primer sequences are listed in Supplementary Material, Table S1. The exon regions corresponding to *Dfnb31* mutations and whirlin protein functional domains are shown at the top and bottom, respectively. (**C**) Summary of RT–PCR results showing disruption of *Dfnb31* mRNA variant expressions in $Dfnb31^{neo/neo}$ (neo) and $Dfnb31^{wi/wi}$ (wi) mice. *Dfnb31* mRNA variant expressions were complex and different in the wild-type (wt) retina and cochlea, and they were differentially disrupted in $Dfnb31^{neo/neo}$ and $Dfnb31^{wi/wi}$ mice. +, presence; –, absence; T, truncated. (**D**) *Dfnb31* variant 8 was intact in the $Dfnb31^{neo/neo}$ cochlea, and *Dfnb31* variants 1–4 and 8 were truncated in all tested tissues of $Dfnb31^{wi/wi}$ mice. Other *Dfnb31* variants were all disrupted in $Dfnb31^{neo/neo}$ and $Dfnb31^{wi/wi}$ mice.

the *Dfnb31*$^{neo/neo}$ cochlea (Fig. 1D), and truncated N-whirlin protein in the *Dfnb31*$^{wi/wi}$ cochlea (Fig. 1D). Although whirlin was previously localized to the ankle link complex (the base) and the tip of stereocilia in both cochlear hair cells (11,13,23,25–27), it was unclear which whirlin isoforms were located in these two subcellular regions and how *Dfnb31* mutations affect their localizations.

To address these, we generated and validated polyclonal antibodies from rabbit, Rb_WHRN_N and Rb_WHRN_C antibodies, which specifically detected whirlin N- and C-terminal regions, respectively (Fig. 1A and Supplementary Material, Fig. S1). By immunofluorescence of P4 cochlear whole-mounts, we found that the immunoreactivity of Rb_WHRN_N was at both stereociliary tips and bases in inner hair cell (IHC) bundles and only at stereociliary bases in outer hair cell (OHC) bundles of wild-type mice (Fig. 2A and Supplementary Material, Fig. S2). The immunoreactivity of Rb_WHRN_N was absent in both *Dfnb31*$^{neo/neo}$ and *Dfnb31*$^{wi/wi}$ IHC and OHC stereocilia (Fig. 2A and Supplementary Material, Fig. S2). Notably, some Rb_WHRN_N signals were found along the kinocilium in IHC and OHC bundles of wild-type and *Dfnb31*$^{wi/wi}$ but not *Dfnb31*$^{neo/neo}$ mice (Fig. 2A and Supplementary Material, Fig. S2), which could be non-specific in the wild-type and truncated N-whirlin fragments in *Dfnb31*$^{wi/wi}$ mutants. The immunoreactivity of Rb_WHRN_C was detected at both stereociliary tips and bases in wild-type IHCs and OHCs (Fig. 2B and Supplementary Material, Fig. S3), and was also localized at the stereociliary tips in *Dfnb31*$^{neo/neo}$ IHCs and OHCs (Fig. 2B and Supplementary Material, Fig. S3). No Rb_WHRN_C signals were detected in *Dfnb31*$^{wi/wi}$ IHCs and OHCs (Fig. 2B and Supplementary Material, Fig. S3). These findings of WHRN_N and WHRN_C immunostaining were consistently observed across the entire cochleas. Careful examination of whirlin immunostaining images also revealed that whirlin appeared to be present at the tip of only the tallest row of stereocilia and at the ankle link complex of several rows of stereocilia in the bundle (Fig. 2). In summary, during development, FL-whirlin is present at stereociliary tips and ankle link complexes of IHCs and only at stereociliary ankle link complexes of OHCs, while C-whirlin is at stereociliary tips of both IHCs and OHCs (Fig. 10C). In *Dfnb31*$^{neo/neo}$ cochleas, C-whirlin is intact at stereociliary tips, while FL-whirlin is disrupted (Fig. 10C). In *Dfnb31*$^{wi/wi}$ cochleas, truncated N-whirlin may be localized along the kinocilium.

Immunofluorescence of cochlear whole-mounts was also conducted at P60 to localize whirlin isoforms in mature hair cells (Fig. 3). At this time point, most stereociliary bundles of *Dfnb31*$^{wi/wi}$ IHCs and OHCs were severely degenerated. Thus, we did not include *Dfnb31*$^{wi/wi}$ mice in this experiment. Rb_WHRN_C antibody detected immunoreactivities only at stereociliary tips in wild-type and *Dfnb31*$^{neo/neo}$ IHCs but not OHCs (Fig. 3A). Furthermore, Rb_WHRN_N antibody detected immunoreactivities at stereociliary tips of wild-type but not *Dfnb31*$^{neo/neo}$ IHCs (Fig. 3B). These findings indicate that whirlin protein localization in mature cochlear hair cells is different from that in developing cochlear hair cells. Both FL-whirlin and C-whirlin are present at IHC but not OHC stereociliary tips in adult wild-type cochleas (Fig. 10C), and C-whirlin is intact at IHC stereociliary tips of mature *Dfnb31*$^{neo/neo}$ cochleas (Fig. 10C).

Morphological, molecular and functional defects of *Dfnb31*$^{neo/neo}$ and *Dfnb31*$^{wi/wi}$ cochlear stereociliary bundles

With the knowledge of differential disruptions of whirlin protein isoforms in *Dfnb31*$^{neo/neo}$ and *Dfnb31*$^{wi/wi}$ mice, we decided to decipher the functions of various whirlin isoforms in the cochlea and understand the pathology of *Dfnb31*$^{neo/neo}$ and *Dfnb31*$^{wi/wi}$ mice by analyzing and comparing their cochlear stereociliary bundle morphology, expression of whirlin-interacting proteins, and hearing function. We examined the stereociliary bundle morphology of *Dfnb31*$^{neo/neo}$ and *Dfnb31*$^{wi/wi}$ cochleas at P4 using scanning electron microscopy (SEM). At a low magnification (Fig. 4A), the stereociliary bundles of OHCs were observed to change from a sharp V- or W-shape to a U-shape in both mutants. Because only FL-whirlin was the isoform disrupted in both *Dfnb31*$^{neo/neo}$ and *Dfnb31*$^{wi/wi}$ cochleas, the similar changes in the OHC bundle shape of the two mutant mice suggest that FL-whirlin at the OHC ankle link complex is involved in maintaining the sharp V- or W-shape of bundles. Due to the normal shallow U-shape of wild-type IHC bundles at this age, we could not tell obvious changes in the shape of two mutant IHC bundles except the frequently observed ectopic stereocilia at the neural side of *Dfnb31*$^{wi/wi}$ IHC stereociliary bundles (Fig. 4C, arrows). We observed more than three rows of stereocilia in both *Dfnb31*$^{neo/neo}$ and *Dfnb31*$^{wi/wi}$ IHCs (Fig. 4C), which could result from loss of FL-whirlin at stereociliary tips and/or ankle link complexes. At a high magnification which permitted visualization of individual stereocilia, we found short and thick stereocilia in *Dfnb31*$^{wi/wi}$ IHCs and OHCs as reported previously (Fig. 4B and C) (21,28,29). However, *Dfnb31*$^{neo/neo}$ stereocilia appeared to have normal length in both IHCs and OHCs and looked thicker in IHCs and normal in OHCs (Fig. 4B and C). Measurement and quantification of stereociliary length (Fig. 5A and B) and thickness (data prepared in another manuscript) in the middle turn of P4 wild-type, *Dfnb31*$^{neo/neo}$ and *Dfnb31*$^{wi/wi}$ cochleas confirmed this impression. We also examined cochlear stereociliary length of P45 *Dfnb31*$^{neo/neo}$ and *Dfnb31*$^{wi/wi}$ mice using the same approach (Fig. 5C and D). We found that both *Dfnb31*$^{wi/wi}$ and *Dfnb31*$^{neo/neo}$ stereocilia were shorter than wild-type stereocilia in IHCs. The *Dfnb31*$^{wi/wi}$ IHC stereocilia became even shorter at this age, compared with those at P4, suggesting that the *Dfnb31*$^{wi/wi}$ IHC stereocilia are unable to maintain their length. In OHCs, the *Dfnb31*$^{wi/wi}$ stereociliary length was shorter, while the *Dfnb31*$^{neo/neo}$ stereociliary length was normal. These findings indicate that C-whirlin at stereociliary tips is sufficient for normal stereociliary length of developing hair cells and mature OHCs, while both FL- and C-whirlins at stereociliary tips are required for normal stereociliary length of mature IHCs.

Whirlin was previously shown to be transported by myosin XVa to the stereociliary tip, where whirlin is proposed to participate in stereociliary elongation by interacting with EPS8 and myosin XVa (11,30). We first confirmed the colocalization of whirlin and EPS8 at stereociliary tips of IHCs and OHCs by double immunofluorescence (Supplementary Material, Fig. S4B). We then analyzed the amounts of EPS8 and myosin XVa proteins at stereociliary tips in the middle turn of P4 *Dfnb31*$^{neo/neo}$ and *Dfnb31*$^{wi/wi}$ cochleas by measuring the intensities of their immunofluorescent signals (Fig. 6A). EPS8 protein of IHCs/OHCs and myosin XVa protein of OHCs were decreased in both whirlin mutant mice with *Dfnb31*$^{wi/wi}$ mice having the lowest levels, whereas myosin XVa protein of IHCs was increased in *Dfnb31*$^{neo/neo}$ and decreased in *Dfnb31*$^{wi/wi}$ mice. This result suggests that both FL-whirlin and C-whirlin are required to maintain the normal amount of EPS8 and myosin XVa at the stereociliary tip of cochlea hair cells. Because of the normal stereociliary length of *Dfnb31*$^{neo/neo}$ cochlear hair cells and the short stereociliary length of *Dfnb31*$^{wi/wi}$ cochlear hair cells observed by SEM at P4, our result also suggests that the amounts of EPS8 and myosin XVa at stereociliary tips may not strictly correlate with stereociliary length. We next studied the interactions of FL-whirlin

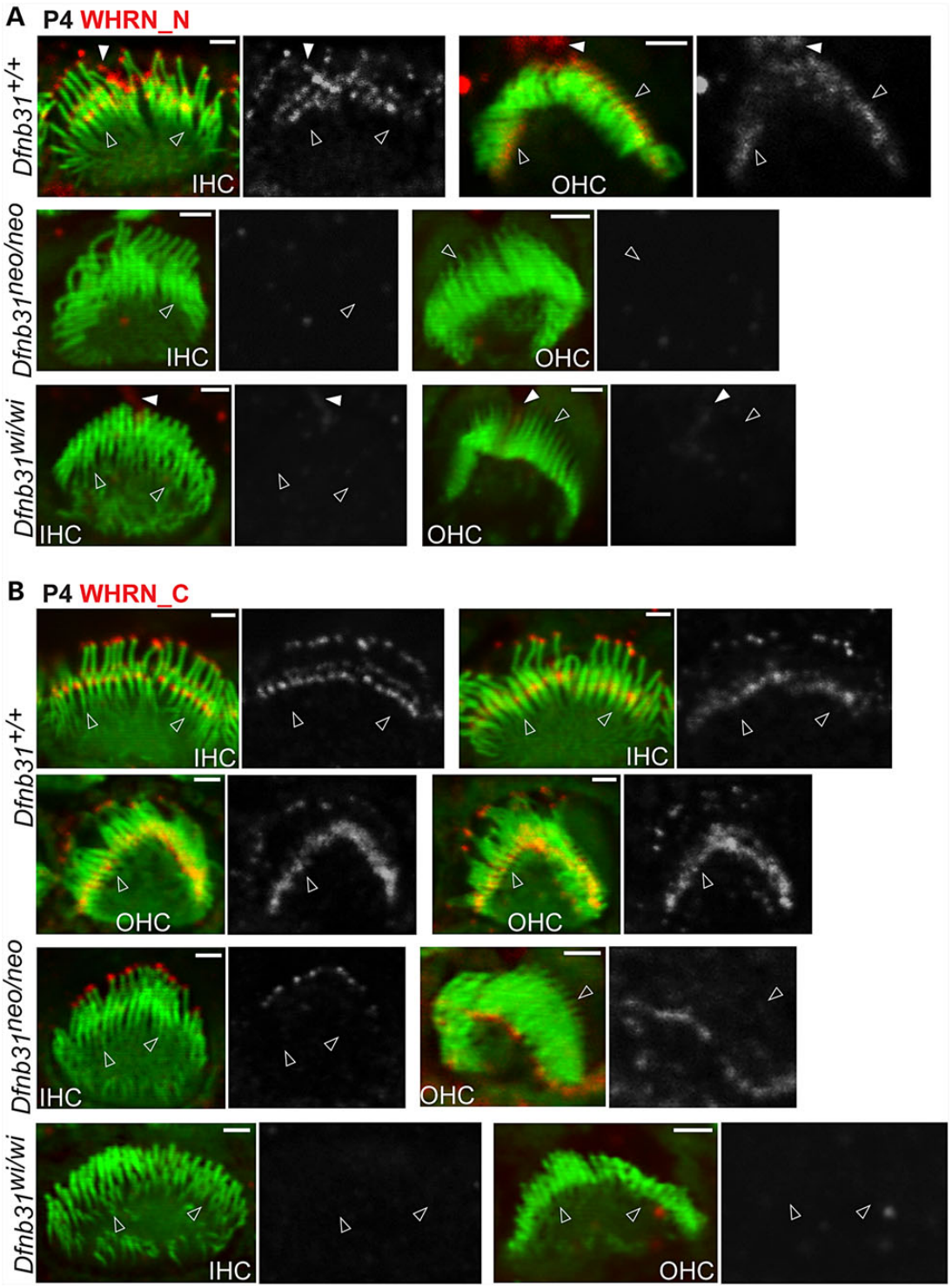

Figure 2. Whirlin protein localization in developing wild-type, *Dfnb31*$^{neo/neo}$ and *Dfnb31*$^{wi/wi}$ cochlear hair cells. (**A**) Immunostaining using rabbit WHRN_N antibody shows signals at the tip and base of IHC stereocilia and only at the base of OHC stereocilia in P4 wild type mice. The same experimental procedure detected no signals in P4 *Dfnb31*$^{neo/neo}$ and *Dfnb31*$^{wi/wi}$ cochlear stereocilia. Note that rabbit WHRN-N antibody also detected signals along the kinocilium in P4 wild-type and *Dfnb31*$^{wi/wi}$ cochlear hair cells (white filled arrows). (**B**) Immunofluorescence using rabbit WHRN_C antibody shows signals at the tip and base of both IHC and OHC stereocilia in P4 wild-type mice. In P4 *Dfnb31*$^{neo/neo}$ IHCs and OHCs, immunoreactivity of rabbit WHRN_C antibody was found at the stereociliary tip. No immunoreactivity of WHRN_C antibody was detected in P4 *Dfnb31*$^{wi/wi}$ cochlear stereociliary bundles. Empty arrows point to stereociliary bases. The red signals of whirlin proteins are shown in grayscale on the right of each overlay panel with the matched position of arrows. Red signals outside stereociliary bundles are non-specific. Scale bars, 1 μm.

(variant 2), C-whirlin (variant 8), and truncated N-whirlin (truncated variant 2 in *Dfnb31*$^{wi/wi}$) proteins with EPS8 and myosin XVa using their recombinant proteins expressed in mammalian cultured cells (Fig. 6B–D). We found that EPS8 was able to be coimmunoprecipitated with FL-whirlin, C-whirlin and truncated N-whirlin at a similar level (Fig. 6C) and that myosin XVa was able

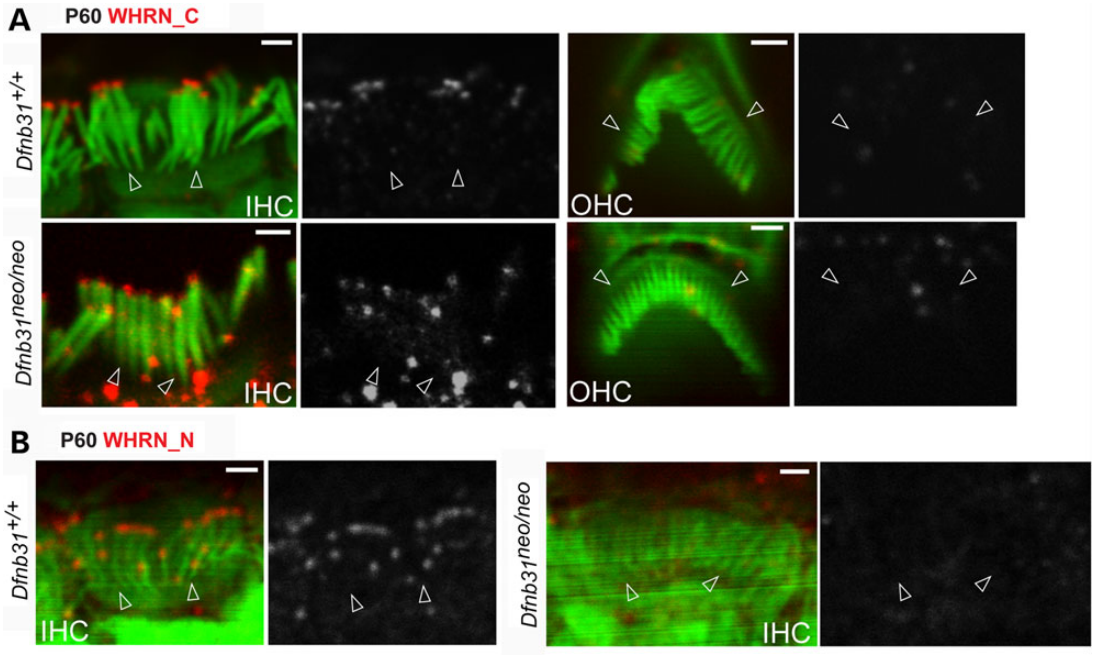

Figure 3. Whirlin protein localization in mature wild-type and *Dfnb31*$^{neo/neo}$ cochlear hair cells. (**A**) The rabbit WHRN_C antibody detected immunoreactivities at IHC but not OHC stereociliary tips of both wild-type and *Dfnb31*$^{neo/neo}$ mice at P60. (**B**) Immunostaining using rabbit WHRN_N antibody revealed immunoreactivities at IHC stereociliary tips of wild-type but not *Dfnb31*$^{neo/neo}$ mice at P60. Empty arrows point to stereociliary bases. The red signals of whirlin proteins are shown in grayscale on the right of each overlay panel with the matched position of arrows. Red signals outside stereociliary bundles are non-specific. Scale bars, 1 μm.

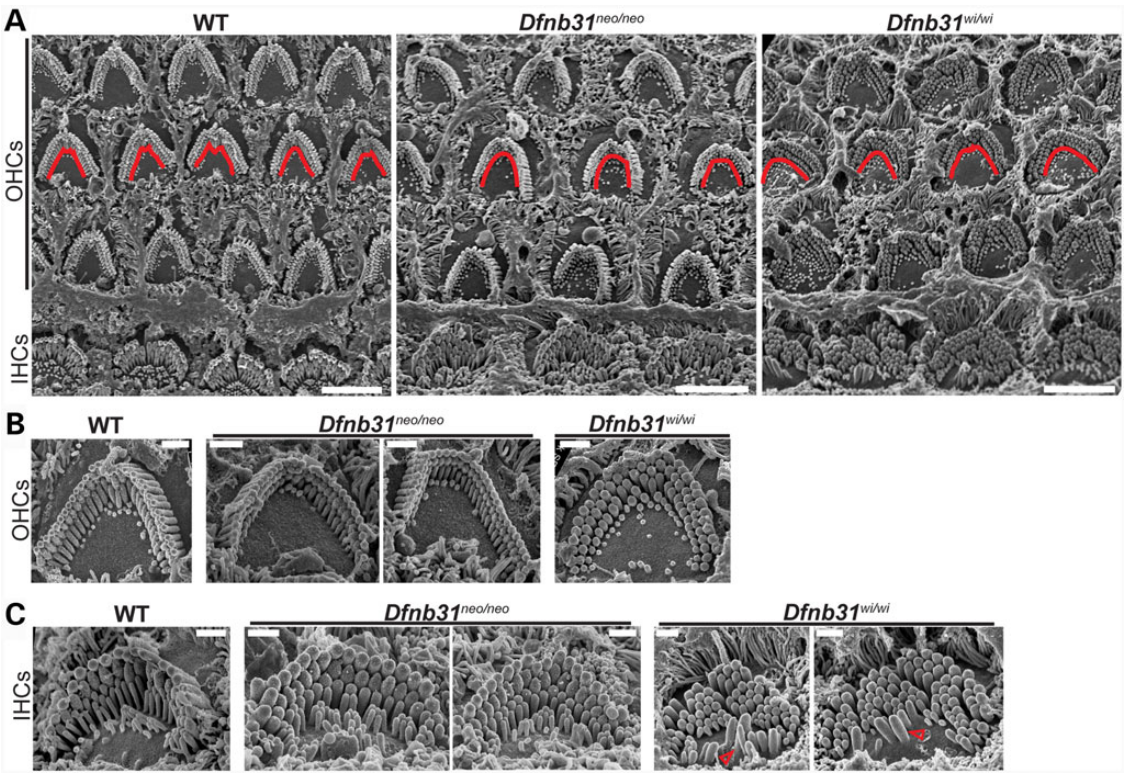

Figure 4. *Dfnb31*$^{wi/wi}$ cochlear stereociliary bundles have more severe morphological defects than *Dfnb31*$^{neo/neo}$ cochlear stereociliary bundles. (**A**) Low-magnification SEM images of wild-type, *Dfnb31*$^{neo/neo}$ and *Dfnb31*$^{wi/wi}$ cochlear stereociliary bundles. *Dfnb31*$^{neo/neo}$ and *Dfnb31*$^{wi/wi}$ OHC stereociliary bundles (traced by red lines) were altered to the U-shape from the V- or W-shape in wild-types. (**B**) Images of individual OHC stereociliary bundles from the cochlear middle turn. In addition to the bundle shape change, stereocilia in *Dfnb31*$^{wi/wi}$ mice were short and thick. (**C**) Images of individual IHC stereociliary bundles from the cochlear middle turn. Compared with wild-type mice, the IHC stereocilia of *Dfnb31*$^{neo/neo}$ and *Dfnb31*$^{wi/wi}$ mice were thick and frequently had more than three rows. Furthermore, *Dfnb31*$^{wi/wi}$ stereocilia were short, and ectopic stereocilia outside *Dfnb31*$^{wi/wi}$ stereociliary bundles (red arrows) were often seen. All images are from P4 animals. Scale bars, 5 μm in (A) and 1 μm in (B) and (C).

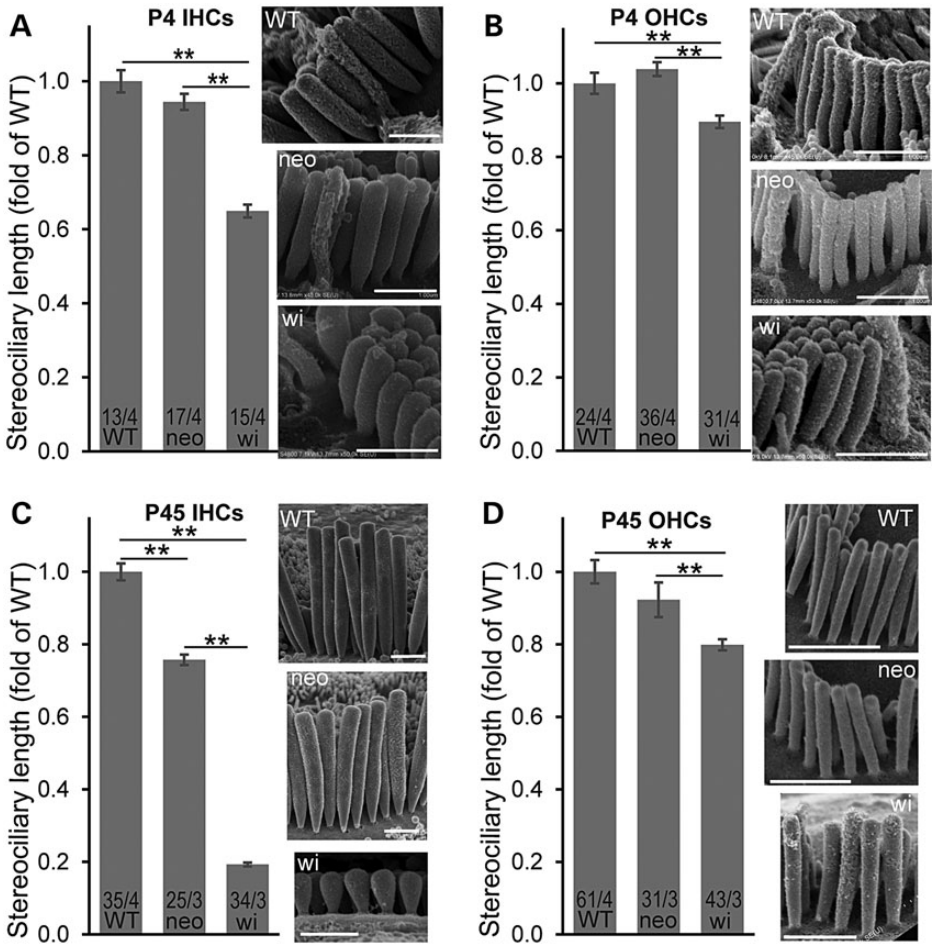

Figure 5. Measurement of stereociliary lengths in *Dfnb31*$^{neo/neo}$ and *Dfnb31*$^{wi/wi}$ cochlear hair cells. (**A** and **B**) *Dfnb31*$^{wi/wi}$ (wi) but not *Dfnb31*$^{neo/neo}$ (neo) mice at P4 had short stereocilia in IHCs (**A**) and OHCs (B). (**C**) Both *Dfnb31*$^{wi/wi}$ and *Dfnb31*$^{neo/neo}$ mice at P45 had short stereocilia in IHCs, although *Dfnb31*$^{neo/neo}$ IHC stereocilia were longer than *Dfnb31*$^{wi/wi}$ IHC stereocilia. (**D**) *Dfnb31*$^{wi/wi}$ but not *Dfnb31*$^{neo/neo}$ mice at P45 had short stereocilia in OHCs. Representative SEM images of stereocilia from each genotype at P4 and P45 are shown on the right of bar charts. Stereocilia in the longest row next to the kinocilium at P4 or in the middle of the row at P45 were measured. Numbers of cells and mice analyzed are listed in the bottom of bars before and after slashes, respectively. Student's t-tests (two-tail) were performed. Error bars, standard error of the mean. $^{**}P < 0.01$.

to be coimmunoprecipitated only with FL-whirlin and C-whirlin but not truncated N-whirlin (Fig. 6D). These results demonstrate that both N- and C-whirlin regions are involved in binding to EPS8, while only C-whirlin region associates with myosin XVa.

In addition, we assessed OHC function by measuring distortion product otoacoustic emissions (DPOAEs) and determined audibility curves using the auditory brainstem responses (ABRs) in *Dfnb31* mutant mice at P45-P60. In these experiments, we included *Dfnb31*$^{wi/neo}$ mice by crossing *Dfnb31*$^{neo/neo}$ and *Dfnb31*$^{wi/wi}$ mice, which presumably express C-whirlin from the *Dfnb31*^{neo} allele and truncated N-whirlin from the *Dfnb31*^{wi} allele, but not FL-whirlin. DPOAE thresholds were significantly elevated by at least 30 dB SPL above control animals for *Dfnb31*$^{wi/neo}$, *Dfnb31*$^{neo/neo}$ and *Dfnb31*$^{wi/wi}$ mice across all frequencies (8–32 kHz), but there was no significant difference in the DPOAE thresholds among the three whirlin mutants (Fig. 7A). These results indicate that OHCs of these mutants had similar functional deficits despite varying stereociliary lengths (Fig. 5B and D) and thicknesses (28,31) across genotypes. These OHC functional deficits probably resulted from abnormal stereociliary bundle shapes (Fig. 4A) caused by FL-whirlin loss, which is shared among the three whirlin mutant mice. However, the three whirlin mutant mice displayed different ABR threshold increases (Fig. 7B). *Dfnb31*$^{wi/wi}$ mice exhibited the most severe hearing loss, while *Dfnb31*$^{wi/neo}$ and *Dfnb31*$^{neo/neo}$ mice showed similar degrees of moderate hearing loss with *Dfnb31*$^{wi/neo}$ mice slightly better at the frequency of 5.6 kHz. The better hearing function of *Dfnb31*$^{neo/neo}$ mice than *Dfnb31*$^{wi/wi}$ mice is similar to that reported in USH2D and *DFNB31* patients (14,19). Because both IHCs and OHCs contribute to ABR measures, we believe that the difference in ABR threshold increases between *Dfnb31*$^{wi/wi}$ and *Dfnb31*$^{wi/neo}$/*Dfnb31*$^{neo/neo}$ mice resulted from differential IHC dysfunctions due to differences in C-whirlin expression. The moderate to severe hearing loss in *Dfnb31*$^{neo/neo}$ and *Dfnb31*$^{wi/neo}$ mice indicates a partial role of C-whirlin and the importance of FL-whirlin in hearing, respectively. Furthermore, the similarity of hearing loss between *Dfnb31*$^{wi/neo}$ and *Dfnb31*$^{neo/neo}$ mice indicates that the truncated N-whirlin present in *Dfnb31*$^{wi/neo}$ mice probably plays a minor role in hearing. In summary, it is the stereociliary bundle shape controlled by FL-whirlin but not the stereociliary length controlled by C-whirlin that is essential for normal OHC-mediated DPOAE; and it is the stereociliary length and three-row stereociliary arrangement controlled by both FL-whirlin and C-whirlin that is critical for the IHC function.

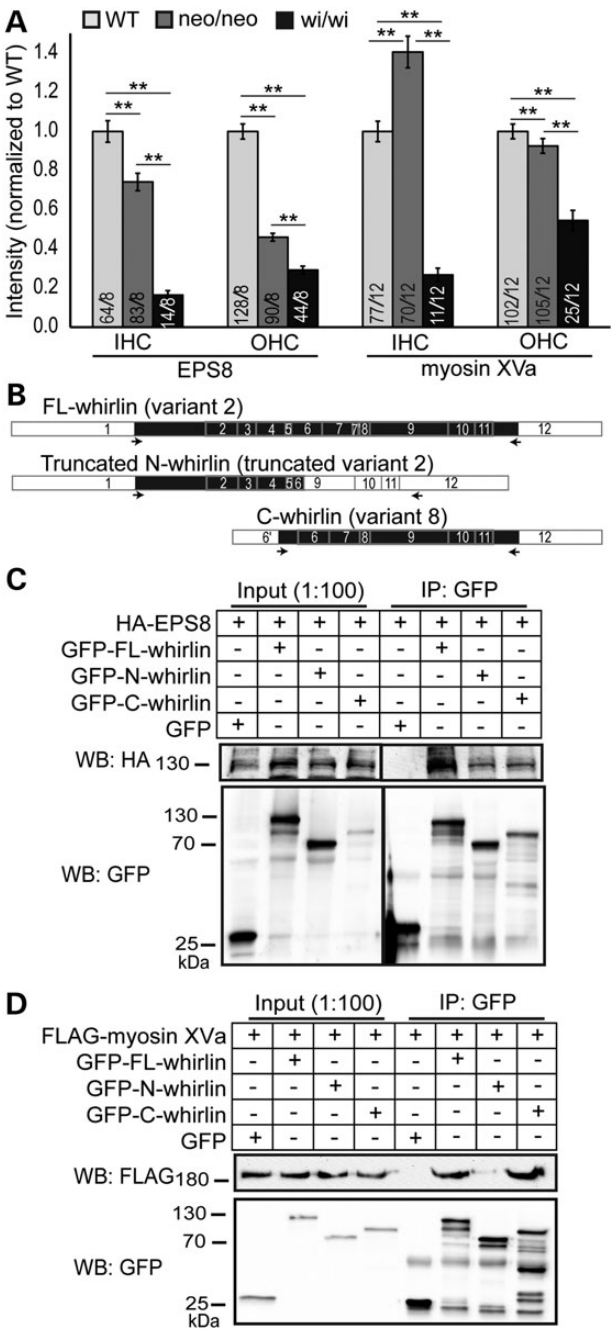

Figure 6. EPS8 and myosin XVa expressions in *Dfnb31*$^{neo/neo}$ and *Dfnb31*$^{wi/wi}$ cochlear hair cells and their interactions with whirlin fragments. (**A**) Quantification of EPS8 and myosin XVa expressions in wild-type (WT), *Dfnb31*$^{neo/neo}$ (neo/neo) and *Dfnb31*$^{wi/wi}$ (wi/wi) mice. EPS8 expression was reduced at the IHC and OHC stereociliary tip of both *Dfnb31*$^{neo/neo}$ and *Dfnb31*$^{wi/wi}$ mice. EPS8 expression was less in *Dfnb31*$^{wi/wi}$ hair cells than in *Dfnb31*$^{neo/neo}$ hair cells. Myosin XVa expression was increased in IHC stereocilia but decreased in OHC stereocilia of *Dfnb31*$^{neo/neo}$ mice, while myosin XVa expression was reduced in both IHC and OHC stereocilia of *Dfnb31*$^{wi/wi}$ mice. Numbers of cells and mice analyzed are shown in the bottom of each bar before and after slashes, respectively. Error bars represent standard error of the mean. Student's *t*-tests (two-tail) were performed. $^{**}P < 0.01$. (**B**) Schematic diagram of whirlin protein fragments used in the coimmunoprecipitation experiments shown in (C) and (D). Arabic numerals are exon numbers. White and black colors indicate untranslated and protein coding regions, respectively. cDNA fragments flanked by arrows were cloned into the GFP-tagged expression vectors. (**C**) HA-tagged EPS8 protein was able to be coimmunoprecipitated with GFP-tagged FL-whirlin, truncated N-whirlin and C-whirlin. (**D**) FLAG-tagged myosin XVa tail fragment was able to be coimmunoprecipitated with GFP-tagged FL-whirlin and C-whirlin but not the truncated N-whirlin. GFP protein from the empty pEGFP-C vector was used as a negative control. The anti-GFP blots demonstrate the success of immunoprecipitations and the amounts of GFP-tagged proteins pulled down in the experiments.

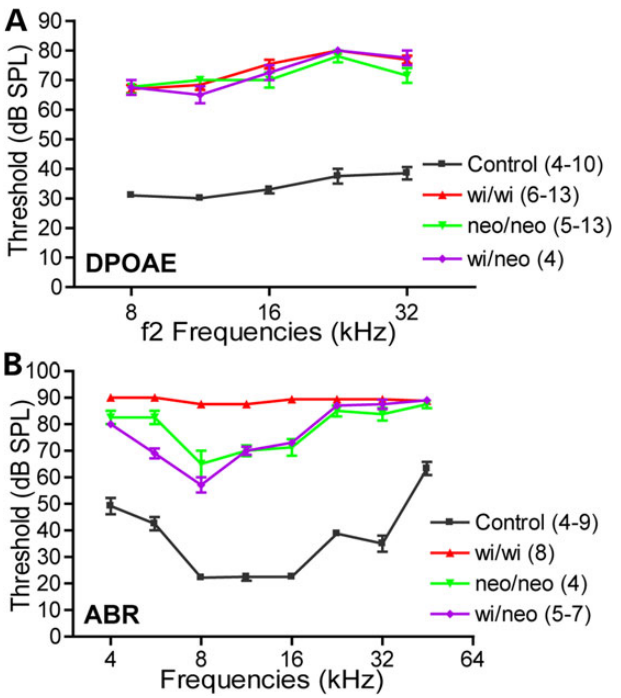

Figure 7. Hearing tests in *Dfnb31*$^{neo/neo}$, *Dfnb31*$^{wi/wi}$ and *Dfnb31*$^{wi/neo}$ mice. (**A**) *Dfnb31*$^{neo/neo}$ (green), *Dfnb31*$^{wi/wi}$ (red) and *Dfnb31*$^{wi/neo}$ (purple) mice exhibited similar DPOAE thresholds in the frequency range of 8–32 kHz at P45-P60. There was no statistically significant difference among the three *Dfnb31* mutant mice ($P > 0.05$). Compared with control mice (black), the thresholds in these three mutant mouse lines were all significantly elevated throughout the tested frequency range ($P < 0.01$). (**B**) *Dfnb31*$^{neo/neo}$, *Dfnb31*$^{wi/wi}$ and *Dfnb31*$^{wi/neo}$ mice displayed different levels of ABR threshold elevation in the frequency range of 4–45 kHz at P45-P60. The thresholds of *Dfnb31*$^{wi/wi}$ mice reached the test ceiling of our ABR system at most tested frequencies. The thresholds of *Dfnb31*$^{neo/neo}$ and *Dfnb31*$^{wi/neo}$ mice were similar to each other except at the frequency of 5.6 kHz. All differences among *Dfnb31*$^{neo/neo}$, *Dfnb31*$^{wi/wi}$ and *Dfnb31*$^{wi/neo}$ mice were statistically significant ($P < 0.01$) except the differences between *Dfnb31*$^{neo/neo}$ and *Dfnb31*$^{wi/neo}$ mice at frequencies of 4, 8, 11.3, 16, 22.6, 32 and 45 kHz. Error bars represent standard error of the mean. Numbers in the legend are the numbers of mice tested in each genotype group. Note that various numbers of mice were tested at different frequencies within the same genotype groups. Two-way ANOVA with Bonferroni correction for multiple comparisons and Student's *t*-tests (two-tail) were performed.

Verification of C-whirlin localization and function in the cochlea of *Dfnb31*$^{tm1a/tm1a}$ and *Dfnb31*$^{wi/wi}$-BAC mice

To verify our findings about the localization and function of whirlin isoforms, we decided to use two more *Dfnb31* mutant mouse lines that were readily available (Fig. 8A and B). *Dfnb31*$^{tm1a/tm1a}$ mice, generated by the European Conditional Mouse Mutagenesis Program (EUCOMM), have a gene trapping cassette in intron 3 (Fig. 8B). The *tm1a* allele was predicted to trap and truncate groups 1 and 4 of *Dfnb31* mRNA variants after exon 3 and to affect expression of these *Dfnb31* variants but not variant 8. Thus, *Dfnb31*$^{tm1a/tm1a}$ mice could be an independent mouse line to verify our findings of *Dfnb31*$^{neo/neo}$ mice. *Dfnb31*$^{wi/wi}$-BAC mice, published previously (18), are *Dfnb31*$^{wi/wi}$ mice carrying a transgenic bacterial artificial chromosome clone, BAC279, which contains

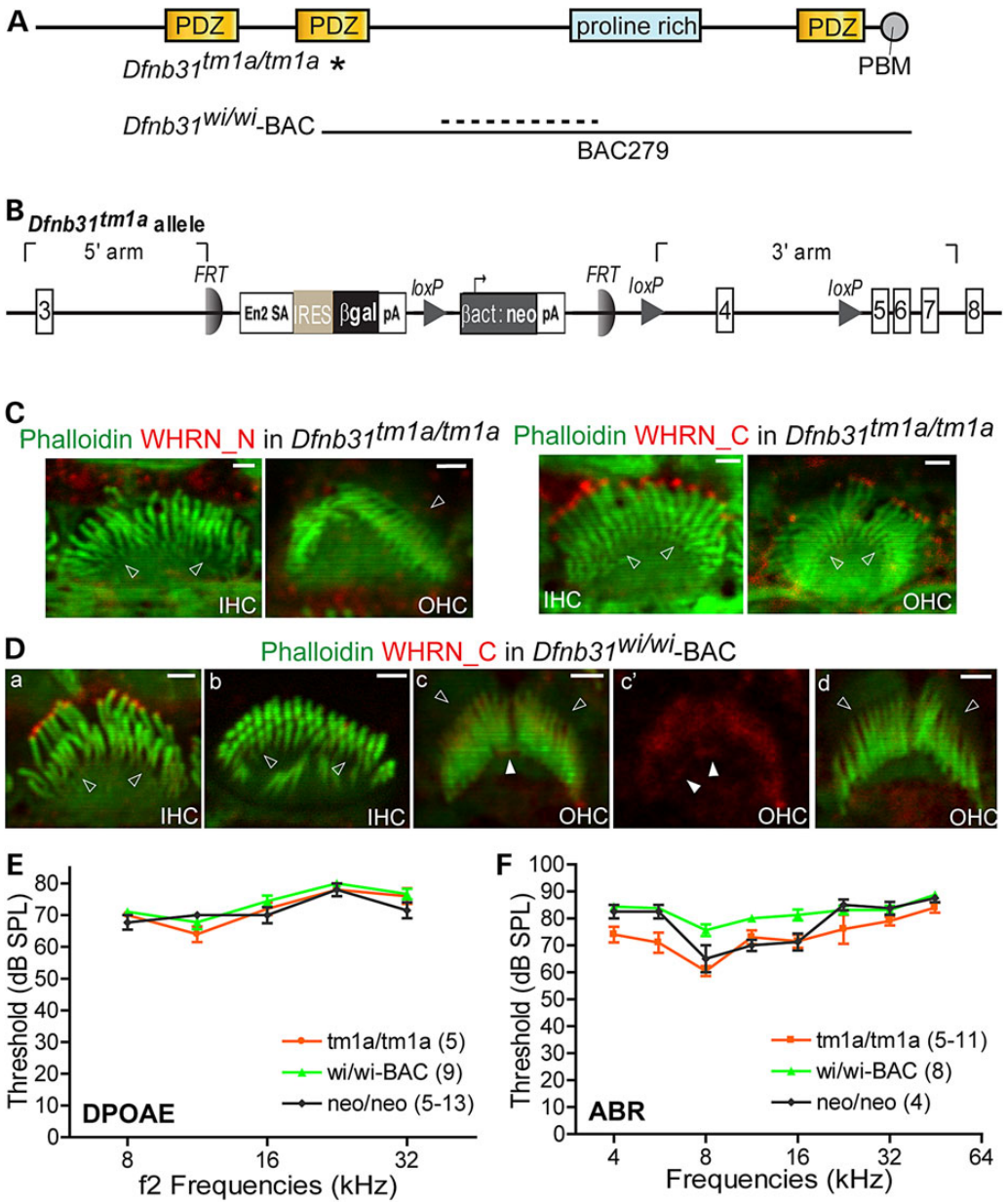

Figure 8. Cochlear phenotypes of *Dfnb31*$^{tm1a/tm1a}$ and *Dfnb31*$^{wi/wi}$-BAC mice are similar to those of *Dfnb31*$^{neo/neo}$ mice. (**A**) Positions of *Dfnb31*$^{tm1a/tm1a}$ (asterisk) and *Dfnb31*$^{wi/wi}$ (dashed line) mutations and the region covered by BAC279 clone (black line) in *Dfnb31*$^{wi/wi}$-BAC mice. (**B**) Detailed scheme of the *Dfnb31*^{tm1a} allele. (**C**) Immunostaining of P4 *Dfnb31*$^{tm1a/tm1a}$ IHCs and OHCs demonstrated no immunoreactivities from rabbit WHRN_N antibody (left) and specific immunoreactivities at stereociliary tips from rabbit WHRN_C antibody (right). (**D**) Immunostaining of P4 *Dfnb31*$^{wi/wi}$-BAC IHCs and OHCs. Whirlin C-terminal signal was detected at stereociliary tips in most (a) but not the rest (b) of IHCs. Some OHCs exhibited whirlin C-terminal signal at the stereociliary base and tip (white arrows in c and c′, c′ is the red channel image of c), while other OHCs showed weak whirlin C-terminal signal only around stereociliary bases (d). Empty arrows in (C) and (D), stereociliary bases; scale bars in (C) and (D), 1 μm. (**E**) DPOAE thresholds of *Dfnb31*$^{tm1a/tm1a}$ and *Dfnb31*$^{wi/wi}$-BAC mice were similar to those of *Dfnb31*$^{neo/neo}$ at P45-P60 ($P > 0.05$). (**F**) ABR thresholds of *Dfnb31*$^{tm1a/tm1a}$ (tm1a/tm1a) and *Dfnb31*$^{wi/wi}$-BAC (wi/wi-BAC) mice were close to those of *Dfnb31*$^{neo/neo}$ (neo/neo) at P45-P60 ($P > 0.05$) except slightly lower ABR thresholds at 5.6 kHz in *Dfnb31*$^{tm1a/tm1a}$ mice ($P < 0.05$) and slightly higher ABR thresholds at 8–16 kHz in *Dfnb31*$^{wi/wi}$-BAC mice ($P < 0.01$). Error bars, SE; numbers in the legend, numbers of mice tested. Two-way ANOVA with Bonferroni correction for multiple comparisons and Student's *t*-tests (two-tail) were performed.

a *Dfnb31* 3′-terminal genomic sequence starting at exon 4 (Fig. 8A). *Dfnb31*$^{wi/wi}$-BAC mice were considered as *Dfnb31*$^{wi/wi}$ mice expressing a C-whirlin fragment (18). To test C-whirlin expression in these two new whirlin mutant mice, we did immunofluorescence of P4 *Dfnb31*$^{tm1a/tm1a}$ and *Dfnb31*$^{wi/wi}$-BAC cochleas. Similar to *Dfnb31*$^{neo/neo}$ mice (Fig. 2), we observed immunoreactivities of Rb_WHRN_C but not Rb_WHRN_N at stereociliary tips of *Dfnb31*$^{tm1a/tm1a}$ IHCs and OHCs (Fig. 8C). In *Dfnb31*$^{wi/wi}$-BAC mice, Rb_WHRN_C immunofluorescent signals were seen in the vast majority of IHCs (Fig. 8Da), while they were absent in ~4% of IHCs. The latter IHCs were mostly distributed in the apical cochlear turn and showed short stereocilia (Fig. 8Db). However, only about 33% of *Dfnb31*$^{wi/wi}$-BAC OHCs displayed Rb_WHRN_C signals at stereociliary tips (Fig. 8Dc and Dc′), and most of these cells were in the apical turn. DPOAE thresholds of *Dfnb31*$^{tm1a/tm1a}$ and *Dfnb31*$^{wi/wi}$-BAC mice were the same as those of *Dfnb31*$^{neo/neo}$ mice at frequencies of 8–32 kHz (Fig. 8E), although most *Dfnb31*$^{wi/wi}$-BAC OHCs did not have C-whirlin at stereociliary tips (Fig. 8Dd). In

general, ABR thresholds were similar among *Dfnb31*$^{tm1a/tm1a}$, *Dfnb31*$^{wi/wi}$-BAC and *Dfnb31*$^{neo/neo}$ mice in the frequency range of 4–45 kHz (Fig. 8F). *Dfnb31*$^{wi/wi}$-BAC mice had slightly worse hearing than the other two mutants at frequencies of 8, 11.3 and 16 kHz, which was probably due to the incomplete expression and localization of C-whirlin at IHC stereociliary tips. *Dfnb31*$^{tm1a/tm1a}$ mice exhibited hearing function slightly better than *Dfnb31*$^{neo/neo}$ mice at the frequency of 5.6 kHz, which could result from their genetic background differences (*Dfnb31*$^{tm1a/tm1a}$: C57BL/6N and *Dfnb31*$^{neo/neo}$: C57BL/6J*129/Sv). Therefore, the findings in *Dfnb31*$^{tm1a/tm1a}$ and *Dfnb31*$^{wi/wi}$-BAC mice are consistent with what we discovered in *Dfnb31*$^{neo/neo}$ mice that C-whirlin in IHC stereociliary tips plays a role in stereociliary elongation and hearing function, while C-whirlin in OHC stereociliary tips may be dispensable for hearing.

Differential disruptions of whirlin expression and function in *Dfnb31*$^{neo/neo}$ and *Dfnb31*$^{wi/wi}$ retinas

Our RT–PCR results (Fig. 1C and D) allowed us to predict that FL-, N- and C-whirlin proteins may exist in wild-type retinas; FL-whirlins may be truncated as truncated N-whirlin fragments in *Dfnb31*$^{wi/wi}$ retinas; and no whirlin proteins exist in *Dfnb31*$^{neo/neo}$ retinas. To verify this, we performed immunoblotting analysis of retinal lysates from wild-type, *Dfnb31*$^{neo/neo}$ and *Dfnb31*$^{wi/wi}$ retinas using Rb_WHRN_N and Rb_WHRN_C antibodies. However, we could not draw any clear conclusions from this experiment because of non-specific bands detected by these two antibodies. Accordingly, we adopted a new approach. We first did immunoprecipitation experiments from retinal lysates of these mice using Rb_WHRN_N and Rb_WHRN_C antibodies and then performed immunoblotting analyses of the immunoprecipitates using chicken WHRN_N and WHRN_C antibodies, respectively (Fig. 9A). In the Rb_WHRN_C immunoprecipitates, no whirlin-specific band was detected except the FL-whirlin in the wild-type retina, suggesting that no C-whirlin is expressed in the wild-type, *Dfnb31*$^{neo/neo}$ or *Dfnb31*$^{wi/wi}$ retinas and no FL-whirlin in the *Dfnb31*$^{neo/neo}$ or *Dfnb31*$^{wi/wi}$ retinas at the protein level. In the Rb_WHRN_N immunoprecipitates, a strong FL-whirlin band was revealed at about 110 kDa in wild-type retinas; a 37-kDa whirlin-specific band was seen in *Dfnb31*$^{wi/wi}$ retinas; and no whirlin-specific band was present in *Dfnb31*$^{neo/neo}$ retinas. To identify the 37-kDa whirlin-specific band in *Dfnb31*$^{wi/wi}$ retinas, gel slices at the 37-kDa position in the wild-type and *Dfnb31*$^{wi/wi}$ lanes were cut and subjected to mass spectrometry. While no whirlin peptides were found in the wild-type sample, 10 whirlin peptides distributed in the N-terminal region of FL-whirlin were identified in the *Dfnb31*$^{wi/wi}$ sample, indicating that the truncated *Dfnb31* variants 1–4 are not subjected to nonsense-mediated mRNA decay and are able to be translated into truncated N-whirlin protein fragments in *Dfnb31*$^{wi/wi}$ retinas (Fig. 9A). Furthermore, an extremely weak whirlin-specific band was observed at about 35 kDa in wild-type but not *Dfnb31*$^{neo/neo}$ or *Dfnb31*$^{wi/wi}$ retinas. Although we did not sequence this band using mass spectrometry, it could be the normal N-whirlin band. Notably, the truncated N-whirlin in *Dfnb31*$^{wi/wi}$ retinas and weak 35-kDa band in wild-type retinas were not observed in our previous study (20), which could be due to the relatively high quality of Rb_WHRN_N antibody generated and used in this study.

To examine the localization of the truncated N-whirlin in *Dfnb31*$^{wi/wi}$ retinas, we conducted immunofluorescence (Fig. 9B). WHRN_N and WHRN_C antibodies were able to detect punctate signals of FL-whirlin and perhaps the low level of N-whirlin at the periciliary membrane complex above the ciliary rootlet in wild-type but not *Dfnb31*$^{neo/neo}$ photoreceptors. In *Dfnb31*$^{wi/wi}$ photoreceptors, we did observe weak WHRN_N but not WHRN_C immunoreactivities above the ciliary rootlet, indicating the truncated N-whirlin fragment was localized normally.

Whirlin was demonstrated to interact with usherin and GPR98, components of the periciliary membrane complex, in photoreceptors (20,24). These interactions are mediated mainly by whirlin N-terminal region (32). Interestingly, immunostaining for GPR98 detected weak signals localized correctly at the periciliary membrane complex in *Dfnb31*$^{wi/wi}$ retinas (Fig. 9C). Considering the previous finding (20) that residual usherin is present in *Dfnb31*$^{wi/wi}$ but not *Dfnb31*$^{neo/neo}$ photoreceptors, we conclude that the truncated N-whirlin fragment is functional in recruiting GPR98 and usherin to the periciliary membrane complex in *Dfnb31*$^{wi/wi}$ retinas, which spares the retina from degeneration. As mentioned above, EPS8 interacts with whirlin at the stereociliary tip of hair cells, and EPS8 expression was reduced in both *Dfnb31*$^{wi/wi}$ and *Dfnb31*$^{neo/neo}$ cochlear hair cells. Therefore, we examined the EPS8 protein expression level in *Dfnb31*$^{neo/neo}$ retinas by immunoblotting and found no significant change in the mutants (Supplementary Material, Fig. S4A).

Discussion

This study presents the first definitive evidence linking differential disruptions of whirlin isoforms to various *Dfnb31* mutations and phenotype manifestations, and suggests an explanation for the genotype–phenotype correlation observed in humans and mice carrying *DFNB31*/*Dfnb31* mutations. We show that *Dfnb31* expression is complex and different in the cochlea and the retina. In these tissues, whirlin isoforms are localized in distinct subcellular compartments and play specific roles. Mutations in different regions of the *Dfnb31* gene disrupt the expression of different whirlin isoforms and lead to hearing loss with or without retinal degeneration in mice, similar to USH2D and *DFNB31* in humans.

Four groups of *Dfnb31* mRNA variants were reported previously in mouse P5 vestibular organs and adult retinas (11,22) with similar *DFNB31* mRNA variants identified in humans (18). Groups 1, 2 and 4 share the same promoter region, but are spliced differently, which results in alternative translation initiation and termination sites. Variants in group 3 have their unique promoter regions. Therefore, the alternative usage of promoters and exons at the transcriptional level as well as the alternative usage of start and stop sites at the translational level provides multiple potential spatial and temporal controls for *Dfnb31* gene expression. For example, the alternative splice sites and promoter used in *Dfnb31* variant 9 could be very weak so that the expression level of this variant is too low to be detected in our experiments (Fig. 1C). Mutations in *Dfnb31*$^{neo/neo}$ and *Dfnb31*$^{tm1a/tm1a}$ mice are positioned in exon 1 and intron 3, respectively. These locations are similar to those of p.Q103X, p.Y228LfsX38, p.A207_K279del, and p.P246HfsX13 mutations in USH2D patients (14,16,17). Our findings from *Dfnb31*$^{neo/neo}$ and *Dfnb31*$^{tm1a/tm1a}$ mice suggest that *DFNB31* variants of groups 1 and 4 but not variant 8 are affected by these mutations in USH2D patients. The affected *DFNB31* variants are probably degraded through nonsense-mediated mRNA decay and cannot be translated into protein fragments with functional domains. By contrast, the *Dfnb31*$^{wi/wi}$ mutation is between exons 6 and 9 at the C-terminal half of whirlin, similar to the mutations of p.R778X and p.G808DfsX11 found in *DFNB31* patients (18,19). Thus, the mutations in *DFNB31* patients could disrupt the same

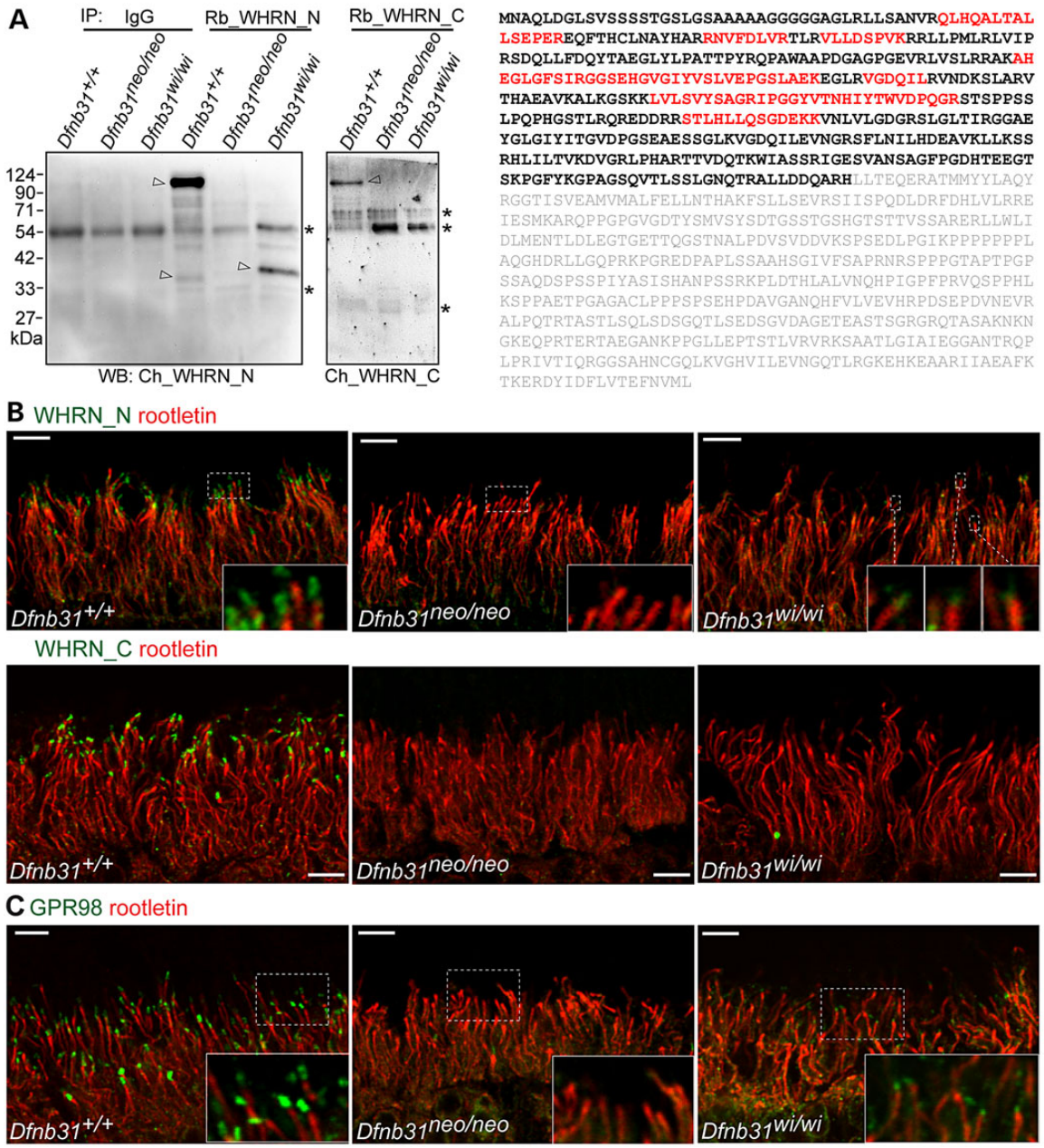

Figure 9. Whirlin protein expression, localization and function in *Dfnb31*$^{neo/neo}$ and *Dfnb31*$^{wi/wi}$ photoreceptors. (**A**) Left, immunoblotting of whirlin immunoprecipitates from adult wild-type, *Dfnb31*$^{neo/neo}$ and *Dfnb31*$^{wi/wi}$ retinas. Arrows point to whirlin-specific bands, and asterisks label the antibody or non-specific bands. IP, immunoprecipitation; WB, immunoblotting; IgG, rabbit immunoglobulin, a negative control; Rb_WHRN_N and Rb_WHRN_C, rabbit antibodies against whirlin N- and C-terminal regions, respectively (Fig. 1A); Ch_WHRN_N and Ch_WHRN_C, chicken antibodies against whirlin N- and C-terminal regions, respectively (Fig. 1A). Right, peptides identified by mass spectrometry are labeled in red in the amino acid sequence of whirlin isoform 2 (NP_001008791). Amino acids labeled in gray are after the *Dfnb31*^{wi} mutation. (**B**) Immunostaining of wild-type, *Dfnb31*$^{neo/neo}$ and *Dfnb31*$^{wi/wi}$ retinas using rabbit WHRN_N (upper row) and WHRN_C (lower row) antibodies. Residual whirlin signals (green) were detected above the ciliary rootlet (rootletin, red) at the periciliary membrane complex in *Dfnb31*$^{wi/wi}$ but not *Dfnb31*$^{neo/neo}$ photoreceptors using the WHRN_N antibody, while no whirlin signals were found in *Dfnb31*$^{neo/neo}$ or *Dfnb31*$^{wi/wi}$ photoreceptors using the WHRN_C antibody. Insets are the amplified view of regions framed by white dashed lines. (**C**) Residual GPR98 signals (green) were detected above the ciliary rootlet (rootletin, red) at the periciliary membrane complex in *Dfnb31*$^{wi/wi}$ but not *Dfnb31*$^{neo/neo}$ photoreceptors. Insets are the enlarged view of GPR98 signals in white boxes. Scale bars, 5 μm.

groups of *DFNB31* mRNA variants as the *Dfnb31*$^{wi/wi}$ mutation and thus generate similar truncated whirlin protein fragments.

Our results demonstrate that *Dfnb31* expresses three main protein isoforms, FL-, C- and N-whirlins, despite the existence of many mRNA variants. In the retina, FL-whirlin and perhaps a low level of N-whirlin are localized to the periciliary membrane complex of photoreceptors, where they were previously shown to interact with usherin and GPR98, the two proteins also associated with USH, in a multiprotein complex (Fig. 10A) (20,24,33). C-whirlin was not observed to be expressed in photoreceptors using immunostaining and pull-down assays. In the inner ear, the localization of whirlin isoforms is hair cell- and time-dependent (Fig. 10C). FL- and C-whirlins are located at stereociliary tips of IHCs, while only C-whirlin is at the OHC stereociliary tips during development. At the stereociliary tip, whirlin isoforms interact with EPS8 and myosin XVa, and contribute to the normal

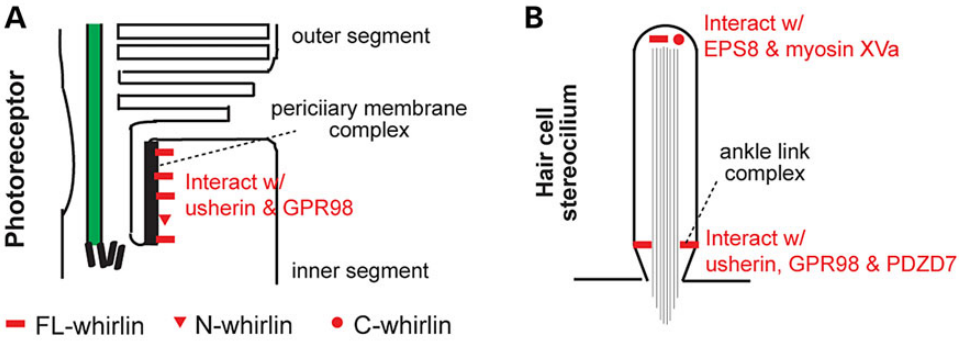

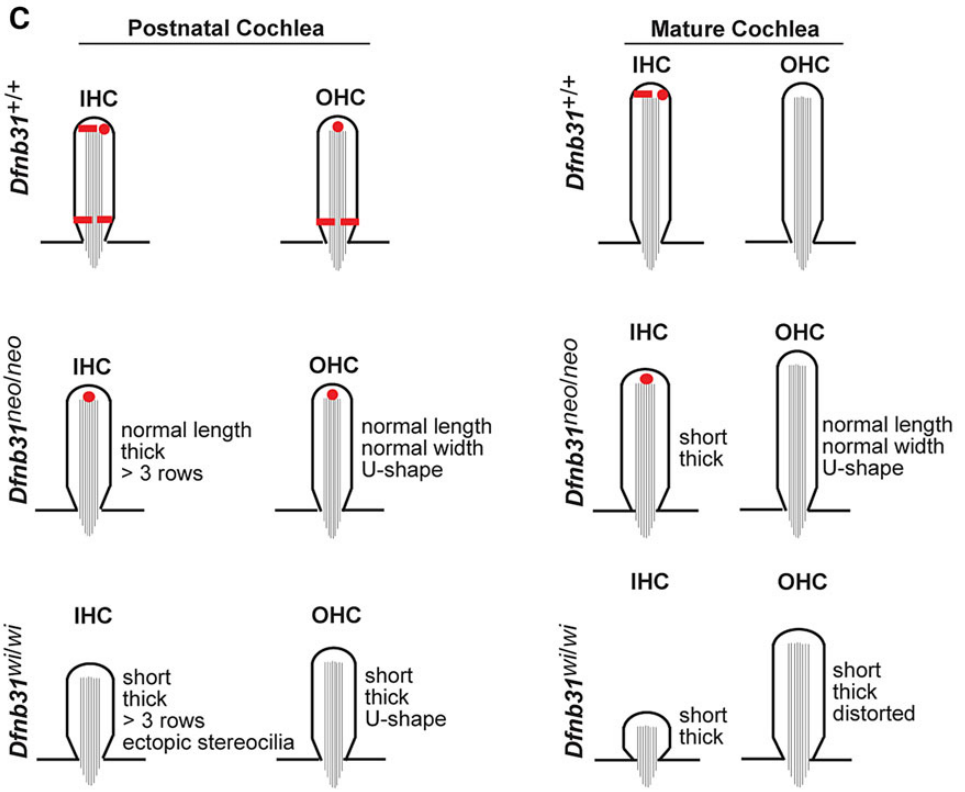

D

	wt	neo/neo	neo/wi	tm1a/tm1a	wi/wi-BAC	wi/wi
DPOAE	+	-	-	-	-	-
ABR	+	-	-	-	-	- -

Figure 10. Summary of localization and function of various whirlin isoforms in photoreceptors and cochlear hair cells. (**A**) FL- and N-whirlins are components of the periciliary membrane complex in photoreceptors. (**B**) In hair cells, FL- and C-whirlins at stereociliary tips interact with EPS8 and myosin XVa for stereociliary elongation, and FL-whirlin at stereociliary bases is a component of the ankle link complex. (**C**) Localization of various whirlin isoforms in the developing and mature cochlear hair cells of wild-type, *Dfnb31*$^{neo/neo}$ and *Dfnb31*$^{wi/wi}$ mice. The changes of stereociliary length and thickness in *Dfnb31*$^{neo/neo}$ and *Dfnb31*$^{wi/wi}$ mice are also shown. (**D**) Results of hearing tests in various whirlin mutant mice. +, normal; –, mildly abnormal; – –, severely abnormal.

stereociliary length in cochlear hair cells (Fig. 10B) (11,30). Only FL-whirlin is present in the ankle link complex at stereociliary bases of cochlear hair cells, where it interacts with usherin, GPR98, and PDZD7 (Fig. 10B) (23,32). Notably, the ankle link complex is a transient structure in cochlear hair cells during development and thus FL-whirlin transiently exists at cochlear stereociliary bases. N-whirlin from group 4 variants probably does not exist in the inner ear. The differential localizations of whirlin isoforms could result from differential localizations of their interacting proteins. For example, the absence of C-whirlin in the ankle link complex is probably due to its lack of N-terminal two PDZ domains, which are known to mediate the interactions between whirlin and ankle link complex components (32).

Previous (20,21,28) and current thorough phenotypical characterizations of various whirlin mutant mice (Fig. 10C) allow us to deduce the functions of various whirlin isoforms in the retina

and cochlea. The absence of retinal degeneration and existence of truncated N-whirlin, usherin, and GPR98 at the correct photoreceptor subcellular compartment in *Dfnb31*$^{wi/wi}$ mice as well as the sequence similarity between the truncated N-whirlin and the normal N-whirlin from group 4 variants indicate that normal N-whirlin may function as FL-whirlin in organizing the periciliary membrane complex of photoreceptors. In the inner ear, the longer stereociliary length in *Dfnb31*$^{neo/neo}$ than in *Dfnb31*$^{wi/wi}$ cochlear hair cells and the presence of C-whirlin at *Dfnb31*$^{neo/neo}$ but not *Dfnb31*$^{wi/wi}$ cochlear stereociliary tips indicate that C-whirlin is indispensable for normal stereociliary length (Fig. 10C). However, the shortening of stereocilia in *Dfnb31*$^{neo/neo}$ mature IHCs indicates that FL-whirlin at stereociliary tips is also required for normal stereociliary length in these cells (Fig. 10C). The shared U-shape phenotypes of *Dfnb31*$^{neo/neo}$ and *Dfnb31*$^{wi/wi}$ OHC bundles imply that the FL-whirlin at the ankle link complex plays a role in the sharp V- or W-shape stereociliary organization of OHCs (Fig. 10C). Furthermore, the stereociliary thickness could be controlled by FL-whirlin at both stereociliary tips and bases of IHCs and by C-whirlin at stereociliary tips of OHCs (Fig. 10C). The three-row stereociliary arrangement of IHC bundles could be related with functions of both FL- and C-whirlins (Fig. 10C).

Surprisingly, our study demonstrates that expression levels of EPS8 and myosin XVa at hair cell stereociliary tips are not closely correlated with stereociliary length, as proposed previously (11,30). Although we observed decreased EPS8 and myosin XVa expressions and short stereocilia in *Dfnb31*$^{wi/wi}$ cochleas as shown in the previous report (30), the changes of EPS8 and myosin XVa expressions at stereociliary tips of *Dfnb31*$^{neo/neo}$ cochleas did not affect stereociliary length at P4. This finding suggests that other proteins may take part in stereociliary elongation and be able to compensate for small changes of EPS8 and myosin XVa expressions. The changes of myosin XVa expression could be compensated by myosin IIIa expression and the emergence of myosin VIIa at stereociliary tips in *Dfnb31*$^{neo/neo}$ mice. Myosin IIIa is known to be able to elongate stereocilia probably through a direct interaction with espin1 at stereociliary tips (34). Myosin VIIa was shown to be present at *Dfnb31*$^{wi/wi}$ stereociliary tips (35) and thus may also localize at *Dfnb31*$^{neo/neo}$ stereociliary tips. The elongation of stereocilia in myosin VIIa mutant mice indicates that myosin VIIa could function in regulation of stereociliary length under some specific circumstances. EPS8L2 belongs to the EPS8 protein family. Its expression complements EPS8 expression spatiotemporally in cochlear hair cells (36) and thus could compensate the small decrease of EPS8 expression in *Dfnb31*$^{neo/neo}$ mice during development.

In addition to understanding the basic scientific question on the roles of whirlin isoforms in hair cell stereociliary development/maintenance and photoreceptor structural maintenance, our study has significant clinical impacts on diagnosis, prognosis, and treatments of hearing loss and vision problems caused by *DFNB31* mutations. Our molecular and cellular investigations of various *Dfnb31* mutations in the mouse cochlea and retina provide convincing evidence for an existence of genotype–phenotype correlation in patients carrying *DFNB31* mutations. This finding allows early accurate diagnosis and prognosis, so that patients are able to be well prepared for their later vision problems and, if available, to receive treatments before the occurrence of vision problems. One patient with a p.Q54X mutation in N-terminal region of *DFNB31* was recently reported to show nonsyndromic retinitis pigmentosa (37). However, this patient self-reported normal hearing and was unavailable for auditory examination in the study. It is possible that the patient may have some level of hearing loss according to another study (16). In that study, a patient with a p.P246HfsX13 mutation in N-terminal region of *DFNB31* had normal hearing by self-report but upon auditory examination displayed a moderate hearing loss. If our prediction is true, the hearing symptom of p.Q54X mutation is consistent with the less severe hearing loss found in *Dfnb31*$^{neo/neo}$ mice (Figs 7B, 8F and 10D). The knowledge of whirlin expression complexity will also help develop effective therapies. For example, AAV-mediated whirlin replacement therapy has been explored in the mouse retina and inner ear (24,38). In these studies, only FL-whirlin was delivered into photoreceptors and hair cells. Although the periciliary membrane complex in photoreceptors and stereociliary morphology in hair cells have been rescued, ABR thresholds are not restored. Our study suggests that delivery of multiple whirlin isoforms may be required to solve this problem. Furthermore, our thorough phenotypical characterizations of various *Dfnb31* mutant mouse models provide valuable information for these models to be used for testing new therapies. Finally, expression of multiple isoforms and causal association with various diseases (e.g. USH versus. DFNB) are two features shared by many USH genes (2). Therefore, disruption of different isoform expressions could be one of the common mechanisms underlying various disease manifestations caused by USH gene mutations.

Materials and Methods

Animals

Dfnb31 targeted mutant (*Dfnb31*$^{neo/neo}$ also known as *Dfnb31*^{tm1Tili}, MGI:4462398), whirler (*Dfnb31*$^{wi/wi}$, MGI:1857090), and *Dfnb31*$^{wi/wi}$ carrying BAC279 (*Dfnb31*$^{wi/wi}$-BAC also known as Tg(Dfnb31)#Ptt, MGI:5616436) mice were described previously (18,20). *Dfnb31*$^{tm1a(EUCOMM)wtsi}$ (MGI:4432119) mice were purchased as frozen sperms from EUCOMM and revived at the University of Utah Transgenic and Gene Targeting mouse core. All experiments involving animals were performed in compliance with the Institutional Animal Care and Use Committee at the University of Utah.

Antibodies and reagents

Two whirlin fragments (1-124 aa and 375-800 aa, NP_082916) were cloned into pET28 vectors, expressed with His tag in BL21-CodonPlus (DE3)-RIPL cells (Agilent Technologies, Santa Clara, CA, USA), and purified by chromatography using Ni^{2+}-charged His•Bind resin (EMD Millipore, Billerica, MA, USA). The other two whirlin fragments (1-472 aa and 721-907 aa, NP_082916) were cloned into pGEX-4T-1 vector, expressed with GST tag in BL21-CodonPlus (DE3)-RIPL cells, and purified by chromatography using glutathione sepharose™ 4 Fast Flow resin (GE Healthcare Life Sciences, Pittsburgh, PA, USA). Purified His-tagged whirlin proteins were applied to immunize rabbits. Antibodies against whirlin were then affinity-purified against the corresponding GST-tagged whirlin fragments. Therefore, the antigen regions of rabbit WHRN_N and WHRN_C antibodies are 1-124 aa and 721-800 aa, respectively. The specificity of purified antibodies was confirmed by immunoblotting of whirlin N- and C-terminal fragments expressed in HEK293 cells (Supplementary Material, Fig. S1). Rabbit GPR98, myosin XVa, and GRP antibodies and chicken whirlin antibodies (WHRN_N aka PDZ350 and WHRN_C aka PDZIE) were described previously (13,20). Antibodies against HA, FLAG, actin, and γ-tubulin (Sigma-Aldrich, St. Louis, MO, USA) and antibody against EPS8 (Santa Cruz Biotechnology, Dallas, TX, USA) were purchased. Alexa fluorochrome-conjugated phalloidin and secondary antibodies were obtained from Life

Technologies (Grand Island, NY, USA). Rabbit immunoglobulin and horseradish peroxidase-conjugated secondary antibodies were from Jackson ImmunoResearch (West Grove, PA, USA).

RNA isolation, RT–PCR, immunoprecipitation, immunoblotting and mass spectrometry

Total RNA was extracted from mouse retinas and cochleas using SurePrep™ RNA Purification Kit (Fisher BioReagents®, Fair Lawn, NJ, USA). RT–PCR was conducted from total RNA using Thermoscript RT–PCR kit (Life Technologies). Manufacturer's instructions were followed exactly during RNA isolation and RT–PCR. EPS8 cDNA fragment (330-2795 bp, NM_001271595) was generated from mouse retinal total RNAs by RT–PCR and inserted into pCMV-HA vector (Clontech Laboratories, Mountain View, CA, USA). Myosin XVa cDNA fragment (2603-7009 bp, NM_182698) was subcloned from a full-length construct (Thomas B. Friedman, NIDCD) into p3XFLAG-Myc-CMV vector (Sigma-Aldrich). Whirlin variant 8 cDNA (311-1963bp, AY739121) was amplified from mouse cochleas by RT–PCR and cloned into pEGFP-C vector (Clontech Laboratories). Truncated N-whirlin fragment was cloned by replacing wild-type whirlin fragment between ppuM1 and BstZ7i sites in FL-whirlin/pEGFP-C vector (31) with the cDNA fragment between the same two sites amplified from *Dfnb31*$^{wi/wi}$ retinas. To study the interactions of EPS8 and myosin XVa with whirlin fragments, HEK293 cells were cotransfected with GFP-tagged whirlin plasmids and either HA-tagged EPS8 plasmid or FLAG-tagged myosin XVa plasmid. Immunoprecipitations of GFP-tagged whirlin fragments were performed from the transfected cell lysates. The presence of EPS8 and myosin XVa in the immunoprecipitates was examined by immunoblotting using antibodies against HA and FLAG, respectively. Immunoprecipitation and immunoblotting were carried out according to our previous descriptions (13,32). For mass spectrometry, immunoprecipitated samples from wild-type and *Dfnb31*$^{wi/wi}$ retinas were run on SDS-PAGE side by side in duplicate. One pair of the samples were subjected to immunoblotting. The gel slices of the other pair of samples were cut on the gel according to the immunoblotting signals and submitted to the Taplin Mass Spectrometry Facility, Harvard Medical School, for protein identification.

Immunofluorescence and SEM

Procedures for immunofluorescence of retinal sections and whole-mount cochlear tissues were the same as previously described (13). Double immunostaining of mouse cochleas for whirlin and EPS8 was first conducted by standard immunofluorescence procedures with rabbit EPS8 antibody and Alexa Fluor® 594 goat anti-rabbit secondary antibody. Subsequently, the cochleas were incubated with 0.45 mg/ml rabbit immunoglobulin for 2 h, washed with PBS, incubated with the biotin-labeled rabbit whirlin antibody in 5% goat serum/PBS overnight, washed with PBS and finally incubated with Alexa Fluor®488-streptavidin for 1 h. Fluorescent images were taken using a confocal laser scanning microscope (Model FV1000, Olympus, Tokyo, Japan). SEM procedures were described previously (13).

Quantification of EPS8 and myosin XVa expressions

In the retina, EPS8 expressions from different genotypes were quantified by measuring EPS8 immunoblotting signal intensities using ImageJ (NIH). The EPS8 signals were normalized using loading control, actin signals, from the same samples. To quantify EPS8 and myosin XVa expressions in the cochlea, tissues from different genotypes were immunostained simultaneously with exactly the same condition to reduce variations. Fluorescent signals were subsequently captured using the same confocal imaging settings. Intensities of EPS8 and myosin XVa immunofluorescence signals were measured at the tip of stereocilia in OHCs and IHCs using ImageJ and subtracted from the background signals at regions next to stereociliary bundles. The EPS8 and myosin XVa expressions in *Dfnb31* mutant mice were normalized by their corresponding expressions in wild-type mice. Quantification of EPS8 and myosin XVa expressions was performed by a person unaware of the genotypes.

Measurement of stereociliary length, ABR and DPOAE

Measurements of cochlear stereociliary lengths were conducted blind to genotype using ImageJ. To measure cochlear stereociliary length, longest stereocilia next to the kinocilium in the stereociliary bundle were chosen in SEM graphs captured from the cochlear middle turn. ABR and DPOAE were tested in mice as previously reported (13).

Statistics

Two-way ANOVA with Bonferroni correction for multiple comparisons was performed using GraphPad Prism 4, to analyze the significance of differences in ABR and DPOAE thresholds among genotypes at various sound frequencies. Student's *t*-tests were conducted using Microsoft Office Excel to compare values, such as stereociliary length and expression level, between two different genotype groups. A *P*-value of <0.05 was considered to indicate a statistically significant difference between groups.

Supplementary Material

Supplementary Material is available at *HMG* online.

Acknowledgements

We thank Masaaki Yoshigi (University of Utah) and Ross Tomaino (Harvard Medical School) for mass spectrometry assistance, Thomas Friedman (NIDCD) for myosin XVa full-length cDNA, and the Wellcome Trust Sanger Institute Mouse Genetics Project (Sanger MGP) and its funders for providing the mutant mice line (Allele: *Dfnb31*$^{tm1a(EUCOMM)wtsi}$).

Conflict of Interest statement. None declared.

Funding

This work was supported by the National Institutes of Health (EY020853 to J.Y., EY014800 to the Department of Ophthalmology &Visual Sciences, University of Utah); Foundation Fighting Blindness (to J.Y.); E. Matilda Ziegler Foundation for the Blind, Inc. (to J.Y.); Research to Prevent Blindness, Inc. (to J.Y. and the Department of Ophthalmology & Visual Sciences, University of Utah); Hearing Health Foundation (to J.Z.); National Organization for Hearing Research Foundation (to J.Z.); and a startup package from the Moran Eye Center, University of Utah (to J.Y.).

References

1. Kimberling, W.J., Hildebrand, M.S., Shearer, A.E., Jensen, M.L., Halder, J.A., Trzupek, K., Cohn, E.S., Weleber, R.G., Stone, E.M. and Smith, R.J. (2010) Frequency of Usher syndrome in two

pediatric populations: implications for genetic screening of deaf and hard of hearing children. *Genet. Med.*, **12**, 512–516.
2. Mathur, P. and Yang, J. (2015) Usher syndrome: hearing loss, retinal degeneration and associated abnormalities. *Biochim. Biophys. Acta.*, **1852**, 406–420.
3. Riazuddin, S., Nazli, S., Ahmed, Z.M., Yang, Y., Zulfiqar, F., Shaikh, R.S., Zafar, A.U., Khan, S.N., Sabar, F., Javid, F.T. *et al.* (2008) Mutation spectrum of MYO7A and evaluation of a novel nonsyndromic deafness DFNB2 allele with residual function. *Hum. Mutat.*, **29**, 502–511.
4. Schultz, J.M., Bhatti, R., Madeo, A.C., Turriff, A., Muskett, J.A., Zalewski, C.K., King, K.A., Ahmed, Z.M., Riazuddin, S., Ahmad, N. *et al.* (2011) Allelic hierarchy of CDH23 mutations causing non-syndromic deafness DFNB12 or Usher syndrome USH1D in compound heterozygotes. *J. Med. Genet.*, **48**, 767–775.
5. Miyasaka, Y., Suzuki, S., Ohshiba, Y., Watanabe, K., Sagara, Y., Yasuda, S.P., Matsuoka, K., Shitara, H., Yonekawa, H., Kominami, R. *et al.* (2013) Compound heterozygosity of the functionally null Cdh23(v-ngt) and hypomorphic Cdh23(ahl) alleles leads to early-onset progressive hearing loss in mice. *Exp. Anim.*, **62**, 333–346.
6. Chen, Z.Y., Hasson, T., Kelley, P.M., Schwender, B.J., Schwartz, M.F., Ramakrishnan, M., Kimberling, W.J., Mooseker, M.S. and Corey, D.P. (1996) Molecular cloning and domain structure of human myosin-VIIa, the gene product defective in Usher syndrome 1B. *Genomics*, **36**, 440–448.
7. Verpy, E., Leibovici, M., Zwaenepoel, I., Liu, X.Z., Gal, A., Salem, N., Mansour, A., Blanchard, S., Kobayashi, I., Keats, B.J. *et al.* (2000) A defect in harmonin, a PDZ domain-containing protein expressed in the inner ear sensory hair cells, underlies Usher syndrome type 1C. *Nat. Genet.*, **26**, 51–55.
8. Ahmed, Z.M., Goodyear, R., Riazuddin, S., Lagziel, A., Legan, P. K., Behra, M., Burgess, S.M., Lilley, K.S., Wilcox, E.R., Griffith, A. J. *et al.* (2006) The tip-link antigen, a protein associated with the transduction complex of sensory hair cells, is protocadherin-15. *J. Neurosci.*, **26**, 7022–7034.
9. Di Palma, F., Pellegrino, R. and Noben-Trauth, K. (2001) Genomic structure, alternative splice forms and normal and mutant alleles of cadherin 23 (Cdh23). *Gene*, **281**, 31–41.
10. Adato, A., Lefevre, G., Delprat, B., Michel, V., Michalski, N., Chardenoux, S., Weil, D., El-Amraoui, A. and Petit, C. (2005) Usherin, the defective protein in Usher syndrome type IIA, is likely to be a component of interstereocilia ankle links in the inner ear sensory cells. *Hum. Mol. Genet.*, **14**, 3921–3932.
11. Belyantseva, I.A., Boger, E.T., Naz, S., Frolenkov, G.I., Sellers, J. R., Ahmed, Z.M., Griffith, A.J. and Friedman, T.B. (2005) Myosin-XVa is required for tip localization of whirlin and differential elongation of hair-cell stereocilia. *Nat. Cell Biol.*, **7**, 148–156.
12. McMillan, D.R., Kayes-Wandover, K.M., Richardson, J.A. and White, P.C. (2002) Very large G protein-coupled receptor-1, the largest known cell surface protein, is highly expressed in the developing central nervous system. *J. Biol. Chem.*, **277**, 785–792.
13. Zou, J., Zheng, T., Ren, C., Askew, C., Liu, X.P., Pan, B., Holt, J.R., Wang, Y. and Yang, J. (2014) Deletion of PDZD7 disrupts the Usher syndrome type 2 protein complex in cochlear hair cells and causes hearing loss in mice. *Hum. Mol. Genet.*, **23**, 2374–2390.
14. Ebermann, I., Scholl, H.P., Charbel Issa, P., Becirovic, E., Lamprecht, J., Jurklies, B., Millan, J.M., Aller, E., Mitter, D. and Bolz, H. (2007) A novel gene for Usher syndrome type 2: mutations in the long isoform of whirlin are associated with retinitis pigmentosa and sensorineural hearing loss. *Hum. Genet.*, **121**, 203–211.
15. Ouyang, X.M., Xia, X.J., Verpy, E., Du, L.L., Pandya, A., Petit, C., Balkany, T., Nance, W.E. and Liu, X.Z. (2002) Mutations in the alternatively spliced exons of USH1C cause non-syndromic recessive deafness. *Hum. Genet.*, **111**, 26–30.
16. Audo, I., Bujakowska, K., Mohand-Said, S., Tronche, S., Lancelot, M.E., Antonio, A., Germain, A., Lonjou, C., Carpentier, W., Sahel, J.A. *et al.* (2011) A novel DFNB31 mutation associated with Usher type 2 syndrome showing variable degrees of auditory loss in a consanguineous Portuguese family. *Mol. Vis.*, **17**, 1598–1606.
17. Besnard, T., Vache, C., Baux, D., Larrieu, L., Abadie, C., Blanchet, C., Odent, S., Blanchet, P., Calvas, P., Hamel, C. *et al.* (2012) Non-USH2A mutations in USH2 patients. *Hum. Mutat.*, **33**, 504–510.
18. Mburu, P., Mustapha, M., Varela, A., Weil, D., El-Amraoui, A., Holme, R.H., Rump, A., Hardisty, R.E., Blanchard, S., Coimbra, R.S. *et al.* (2003) Defects in whirlin, a PDZ domain molecule involved in stereocilia elongation, cause deafness in the whirler mouse and families with DFNB31. *Nat. Genet.*, **34**, 421–428.
19. Tlili, A., Charfedine, I., Lahmar, I., Benzina, Z., Mohamed, B. A., Weil, D., Idriss, N., Drira, M., Masmoudi, S. and Ayadi, H. (2005) Identification of a novel frameshift mutation in the DFNB31/WHRN gene in a Tunisian consanguineous family with hereditary non-syndromic recessive hearing loss. *Hum. Mutat.*, **25**, 503.
20. Yang, J., Liu, X., Zhao, Y., Adamian, M., Pawlyk, B., Sun, X., McMillan, D.R., Liberman, M.C. and Li, T. (2010) Ablation of whirlin long isoform disrupts the USH2 protein complex and causes vision and hearing loss. *PLoS Genet.*, **6**, e1000955.
21. Holme, R.H., Kiernan, B.W., Brown, S.D. and Steel, K.P. (2002) Elongation of hair cell stereocilia is defective in the mouse mutant whirler. *J. Comp. Neurol.*, **450**, 94–102.
22. Wright, R.N., Hong, D.H. and Perkins, B. (2012) RpgrORF15 connects to the usher protein network through direct interactions with multiple whirlin isoforms. *Invest. Ophthalmol. Vis. Sci.*, **53**, 1519–1529.
23. Michalski, N., Michel, V., Bahloul, A., Lefevre, G., Barral, J., Yagi, H., Chardenoux, S., Weil, D., Martin, P., Hardelin, J.P. *et al.* (2007) Molecular characterization of the ankle-link complex in cochlear hair cells and its role in the hair bundle functioning. *J. Neurosci.*, **27**, 6478–6488.
24. Zou, J., Luo, L., Shen, Z., Chiodo, V.A., Ambati, B.K., Hauswirth, W.W. and Yang, J. (2011) Whirlin replacement restores the formation of the USH2 protein complex in whirlin knockout photoreceptors. *Invest. Ophthalmol. Vis. Sci.*, **52**, 2343–2351.
25. Delprat, B., Michel, V., Goodyear, R., Yamasaki, Y., Michalski, N., El-Amraoui, A., Perfettini, I., Legrain, P., Richardson, G., Hardelin, J.P. *et al.* (2005) Myosin XVa and whirlin, two deafness gene products required for hair bundle growth, are located at the stereocilia tips and interact directly. *Hum. Mol. Genet.*, **14**, 401–410.
26. Kikkawa, Y., Mburu, P., Morse, S., Kominami, R., Townsend, S. and Brown, S.D. (2005) Mutant analysis reveals whirlin as a dynamic organizer in the growing hair cell stereocilium. *Hum. Mol. Genet.*, **14**, 391–400.
27. Grati, M., Shin, J.B., Weston, M.D., Green, J., Bhat, M.A., Gillespie, P.G. and Kachar, B. (2012) Localization of PDZD7 to the stereocilia ankle-link associates this scaffolding protein with the Usher syndrome protein network. *J. Neurosci.*, **32**, 14288–14293.
28. Mogensen, M.M., Rzadzinska, A. and Steel, K.P. (2007) The deaf mouse mutant whirler suggests a role for whirlin in actin filament dynamics and stereocilia development. *Cell Motil. Cytoskeleton*, **64**, 496–508.

29. Mustapha, M., Beyer, L.A., Izumikawa, M., Swiderski, D.L., Dolan, D.F., Raphael, Y. and Camper, S.A. (2007) Whirler mutant hair cells have less severe pathology than shaker 2 or double mutants. *J. Assoc. Res. Otolaryngol.*, **8**, 329–337.
30. Manor, U., Disanza, A., Grati, M., Andrade, L., Lin, H., Di Fiore, P.P., Scita, G. and Kachar, B. (2011) Regulation of stereocilia length by myosin XVa and whirlin depends on the actin-regulatory protein Eps8. *Curr. Biol.*, **21**, 167–172.
31. Wang, L., Zou, J., Shen, Z., Song, E. and Yang, J. (2012) Whirlin interacts with espin and modulates its actin-regulatory function: an insight into the mechanism of Usher syndrome type II. *Hum. Mol. Genet.*, **21**, 692–710.
32. Chen, Q., Zou, J., Shen, Z., Zhang, W. and Yang, J. (2014) Whirlin and PDZ Domain Containing 7 (PDZD7) Proteins are Both Required to Form the Quaternary Protein Complex Associated with Usher Syndrome Type 2. *J. Biol. Chem.*, **289**, 36070–36088.
33. van Wijk, E., van der Zwaag, B., Peters, T., Zimmermann, U., Te Brinke, H., Kersten, F.F., Marker, T., Aller, E., Hoefsloot, L. H., Cremers, C.W. *et al.* (2006) The DFNB31 gene product whirlin connects to the Usher protein network in the cochlea and retina by direct association with USH2A and VLGR1. *Hum. Mol. Genet.*, **15**, 751–765.
34. Salles, F.T., Merritt, R.C. Jr, Manor, U., Dougherty, G.W., Sousa, A.D., Moore, J.E., Yengo, C.M., Dose, A.C. and Kachar, B. (2009) Myosin IIIa boosts elongation of stereocilia by transporting espin 1 to the plus ends of actin filaments. *Nat. Cell Biol.*, **11**, 443–450.
35. Prosser, H.M., Rzadzinska, A.K., Steel, K.P. and Bradley, A. (2008) Mosaic complementation demonstrates a regulatory role for myosin VIIa in actin dynamics of stereocilia. *Mol. Cell. Biol.*, **28**, 1702–1712.
36. Furness, D.N., Johnson, S.L., Manor, U., Ruttiger, L., Tocchetti, A., Offenhauser, N., Olt, J., Goodyear, R.J., Vijayakumar, S., Dai, Y. *et al.* (2013) Progressive hearing loss and gradual deterioration of sensory hair bundles in the ears of mice lacking the actin-binding protein Eps8L2. *Proc. Natl. Acad. Sci. USA*, **110**, 13898–13903.
37. Nishiguchi, K.M., Tearle, R.G., Liu, Y.P., Oh, E.C., Miyake, N., Benaglio, P., Harper, S., Koskiniemi-Kuendig, H., Venturini, G., Sharon, D. *et al.* (2013) Whole genome sequencing in patients with retinitis pigmentosa reveals pathogenic DNA structural changes and NEK2 as a new disease gene. *Proc. Natl. Acad. Sci. USA*, **110**, 16139–16144.
38. Chien, W., Isgrig, K., Roy, S., Belyantseva, I.A., Drummond, M., May, L., Fitzgerald, T., Friedman, T.B. and Cunningham, L. (2015) Gene Therapy Restores Hair Cell Stereocilia Morphology in the Whirler Mouse Cochlea. *ARO 38th Annual MidWinter Meeting Abstract Book*, **38**, 268.